Published in final edited form as:
Nat Immunol. 2014 March ; 15(3): 283–293. doi:10.1038/ni.2828.

Stage-specific control of early B cell development by the transcription factor Ikaros

Tanja A. Schwickert[#1], **Hiromi Tagoh**[#1], **Sinan Gültekin**[1], **Aleksandar Dakic**[1,3], **Elin Axelsson**[1], **Martina Minnich**[1], **Anja Ebert**[1], **Barbara Werner**[1], **Mareike Roth**[1], **Luisa Cimmino**[2], **Ross A. Dickins**[2], **Johannes Zuber**[1], **Markus Jaritz**[1], and **Meinrad Busslinger**[1,#]

[1]Research Institute of Molecular Pathology, Vienna Biocenter, Dr. Bohr-Gasse 7, A-1030 Vienna, Austria

[2]The Walter and Eliza Hall Institute of Medical Research, 1G Royal Parade, Parkville, Victoria 3052, Australia

[#] These authors contributed equally to this work.

Abstract

Ikaros is an essential regulator of lymphopoiesis. Here, we studied the B-cell-specific function of Ikaros by conditional *Ikzf1* inactivation in pro-B cells. B-cell development was arrested at an aberrant 'pro-B' cell stage characterized by increased cell adhesion and loss of pre-B cell receptor signaling. Ikaros was found to activate genes coding for pre-BCR signal transducers and to repress genes involved in the downregulation of pre-BCR signaling and upregulation of the integrin signaling pathway. Unexpectedly, derepression of Aiolos expression could not compensate for the loss of Ikaros in pro-B cells. Ikaros induced or suppressed active chromatin at regulatory elements of activated or repressed target genes. Notably, Ikaros binding and target gene expression was dynamically regulated at distinct stages of early B-lymphopoiesis.

Keywords

Ikaros; conditional mutagenesis; pro-B-to-pre-B cell developmental arrest; regulated Ikaros target genes; pre-BCR signaling; cell adhesion; chromatin regulation

[#]To whom correspondence should be addressed: phone: (+43/1) 797 30 – 3150 fax: (+43/1) 797 30 – 223150 busslinger@imp.ac.at.
[3]Present address: The Walter and Eliza Hall Institute of Medical Research, 1G Royal Parade, Parkville, Victoria 3052, Australia

Accession numbers

The RNA-seq and Bio-ChIP-seq data are available at the Gene Expression Omnibus (GEO) repository under the accession numbers GSE53595.

Author Contributions

T.A.S and H.T. did most experiments; S.G. analyzed the *Ikzf1*$^{ihCd2/+}$ mouse and generated the Ikaros ChIP-seq data of pre-pro-B cells; E.A. and M.J. performed the bioinformatic analyses of all RNA- and ChIP-seq data, respectively; M.M. and A.E provided the PU.1 and IRF4 ChIP-seq data, respectively; A.D. and B.W. generated the *Ikzf1*$^{ihCd2/+}$ and *Ikzf*$^{fl/fl}$ mice, respectively; L.C. and R.A.D. characterized the *Ikzf1* shRNAs; M.R. and J.Z. provided advice and help with the shRNA experiments; T.A.S., H.T. and M.B. planned the project, designed the experiments and wrote the manuscript.

Europe PMC Funders Author Manuscripts

Introduction

Ikaros (*Ikzf1*) is the founding member of a small transcription factor family, which is characterized by a central DNA-binding domain consisting of four zinc fingers (F1-F4) and a C-terminal dimerization region containing two additional zinc fingers (F5, F6)1. Although Ikaros is broadly expressed in hematopoietic progenitors and their lineages, it functions primarily as key regulator of lymphopoiesis1. Ikaros-null ($Ikzf1^{-/-}$) mice lacking the C-terminal zinc fingers fail to generate B-lymphocytes, nature killer cells and fetal T-cells, while giving rise to postnatal development of aberrant T-cells2. In humans, heterozygous *IKZF1* mutations are frequently associated with B-cell precursor acute lymphoblastic leukemia (B-ALL) containing the *BCR-ABL1* translocation3. Although *IKZF1* mutations in B-ALL correlate with poor prognosis4, little is yet known about the role of Ikaros in B-ALL and B cell development.

Ikaros is essential for the priming of lymphoid gene expression in multipotent progenitors (MPPs)5. In the absence of Ikaros, MPPs are unable to differentiate to common lymphoid progenitors (CLPs), thus resulting in a stringent arrest prior to B-cell commitment in $Ikzf1^{-/-}$ mice6. B-cells are, however, generated in $Ikzf1^{L/L}$ mice carrying a hypomorphic *Ikzf1* mutation, although their differentiation is severely impaired at all developmental stages7. Notably, the function of the Ikaros DNA-binding zinc fingers F1 and F4 differentially affects B-cell development, as deletion of F1 leads to a severe reduction of pre-B cells and subsequent B-lymphopoiesis in $Ikzf1^{\Delta F1/\Delta F1}$ mice in contrast to the mild B-cell phenotype observed in $Ikzf1^{\Delta F4/\Delta F4}$ mice8.

Productive V_H-DJ_H recombination of the immunoglobulin heavy-chain (*Igh*) locus in pro-B cells leads to expression of the Igμ protein, which forms the pre-B cell receptor together with the surrogate light chains λ5 and VpreB and the signal-transducing chains Igα and Igβ9. Pre-BCR signaling in large pre-B cells leads to cessation of *Igh* recombination, proliferative cell expansion and subsequent differentiation to small pre-B cells undergoing Ig light-chain gene rearrangements9. Pre-BCR signaling also induces expression of the Ikaros family member Aiolos10. Overexpression of Ikaros and Aiolos in cultured B-ALL and pre-B cell lines has implicated the two transcription factors in the termination of pre-BCR signaling and the control of cell cycle exit10–14. In these in vitro experimental settings, Ikaros and Aiolos silenced the expression of λ5 and VpreB10,11 and down-regulated the expression of the cell cycle regulators Myc and cyclin D312,14. Although these findings were recently confirmed and extended by an Ikaros binding and overexpression study in an *Il7* transgenic pre-B cell line15, the in vivo function of Ikaros in early B-cell development is still unknown in the absence of a conditional loss-of-function analysis.

Here, we have studied the role of Ikaros in early B-cell development by conditional mutagenesis and defined the molecular function of Ikaros by identifying regulated Ikaros target genes through genome-wide sequencing approaches. These studies demonstrated that Ikaros stringently controls the pro-B-to-pre-B cell transition by promoting pre-BCR signaling and cell migration, while suppressing cell adhesion.

Results

Ikaros expression throughout B-cell development

To investigate the function of Ikaros in B-cell development, we created two novel *Ikzf1* alleles. The *Ikzf1*^{ihCd2} allele was generated by insertion of a C-terminal biotin acceptor sequence at the last *Ikzf1* codon and an IRES-*hCd2* (ihCD2) reporter gene upstream of the 3' untranslated region of the *Ikzf1* gene (Supplementary Fig. 1a,b). Notably, the *E. coli* biotin ligase BirA efficiently biotinylated the Ikaros-Bio protein in *Ikzf1*$^{ihCd2/+}$ *Rosa26*$^{BirA/BirA}$ pro-B cells (Supplementary Fig. 1c), thus facilitating streptavidin-mediated pulldown of Ikaros-Bio. Moreover, B and T cell development was similar in *Ikzf1*$^{ihCd2/ihCd2}$ *Rosa26*$^{BirA/BirA}$ mice compared to control littermates (Supplementary Fig. 1d). Flow cytometric analysis of *Ikzf1*$^{ihCd2/+}$ knock-in mice demonstrated that *Ikzf1* is highly expressed in hematopoietic progenitors (MPPs, LMPPs and CLPs), throughout B-cell development from pro-B cells to terminally differentiated plasma cells, as well as during T-lymphopoiesis from the earliest thymic T-cell progenitors (DN1) to peripheral T-cells in contrast to its lower expression in erythroblasts, granulocytes and macrophages (Fig. 1a and Supplementary Fig. 1e). Importantly, intracellular Ikaros staining revealed a similar expression pattern of the endogenous Ikaros and hCD2 reporter proteins during B-cell development (Supplementary Fig. 1f,g), indicating that Ikaros protein expression is not posttranscriptionally regulated in B-cells.

Ikaros loss in pro-B cells arrests development at the pro-B-to-pre-B cell transition

For functional studies, we generated a second, floxed (fl) *Ikzf1* allele by inserting *loxP* sites flanking exon 8 (Supplementary Fig. 2a-c), which encodes the two C-terminal zinc fingers responsible for Ikaros dimerization16. Lymphocyte development was normal in homozygous *Ikzf1*$^{fl/fl}$ mice as well as in *Ikzf1*$^{fl/–}$ mice containing the *Ikzf1* null (–) allele2 (Supplementary Fig. 2d,e). As the *Cd79a*-Cre line (also known as *mb1*-Cre line)17 initiates gene deletion at the transition from pre-pro-B to committed pro-B cells18, we used this Cre line to delete the floxed *Ikzf1* allele in B-cells of control *Ikzf1*$^{fl/+}$ mice and experimental *Ikzf1*$^{fl/–}$ littermates. Notably, B-cell-specific deletion of *Ikzf1* did not lead to B-cell leukemia in *Cd79a*-Cre *Ikzf1*$^{fl/–}$ mice during a one-year observation period in contrast to the development of T-cell leukemia in all *Rag2*-Cre *Ikzf1*$^{fl/–}$ and *Il7r*-Cre *Ikzf1*$^{fl/–}$ mice due to *Ikzf1* inactivation in the T-cell lineage (Supplementary Fig. 2f). Flow cytometric analysis of the bone marrow revealed that total B-cells were 6-fold reduced due to an almost complete loss of pre-B cells and all subsequent developmental stages in *Cd79a*-Cre *Ikzf1*$^{fl/–}$ mice compared to control *Cd79a*-Cre *Ikzf1*$^{fl/+}$ littermates (Fig. 1b,c). In contrast, c-Kit^{hi} pro-B cells (c-Kit^{hi}CD19^{+}CD2$^{–}$IgM$^{–}$IgD$^{–}$) were 2-fold increased in the bone marrow of *Cd79a*-Cre *Ikzf1*$^{fl/–}$ mice (Fig. 1b,c), consistent with the fact that the *Ikzf1* allele was efficiently deleted in these pro-B cells (Fig. 1d). In addition to the c-Kit^{hi} pro-B cells, the bone marrow of *Cd79a*-Cre *Ikzf1*$^{fl/–}$ mice contained a second prominent population of c-Kit^{lo} cells (c-Kit^{lo}CD19^{+}CD2$^{–}$IgM$^{–}$IgD$^{–}$) (Fig. 1b,e). With progressing age, the number of these c-Kit^{lo} cells decreased more slowly (1.8-fold) compared to the c-Kit^{hi} pro-B cells (3.7-fold) in *Cd79a*-Cre *Ikzf1*$^{fl/–}$ mice (Fig. 1e). Together, these data identified an essential role of Ikaros in controlling the pro-B-to-pre-B cell transition.

Proliferation defect of *Ikzf1* mutant pro-B cells despite expression of pre-BCR components

Cell cycle analysis revealed that the c-Kit^{hi} pro-B cells (CD19^{+}B220^{+}CD2^{-}IgM^{-}IgD^{-}) proliferated equally well in the bone marrow of *Cd79a*-Cre *Ikzf1*$^{fl/-}$ and control *Cd79a*-Cre *Ikzf1*$^{fl/+}$ littermates (Fig. 2a,b). In contrast, the c-Kit^{lo} cells (CD19^{+}B220^{+}CD2^{-}IgM^{-}IgD^{-}) of the *Cd79a*-Cre *Ikzf1*$^{fl/-}$ mice preferentially accumulated in the G1/0 phase compared to the large cycling c-Kit^{lo} pre-B cells (CD19^{+}B220^{+}CD2^{-}IgM^{-}IgD^{-}) of control *Cd79a*-Cre *Ikzf1*$^{fl/+}$ mice (Fig. 2a,b). Notably, the G1 arrest did not lead to apoptosis and thus an increase of c-Kit^{lo} cells in the sub-G1 cell fraction (Fig. 2a,b). Consistent with these findings, the size of the c-Kit^{lo} cells in *Cd79a*-Cre *Ikzf1*$^{fl/-}$ mice was small in contrast to the large cycling c-Kit^{lo} pre-B cells of control *Cd79a*-Cre *Ikzf1*$^{fl/+}$ littermates (Fig. 2c). Surprisingly, all *Ikzf1* mutant c-Kit^{lo} cells expressed a functionally rearranged Igμ protein similar to the large c-Kit^{lo} pre-B cells of the control genotype (Fig. 2c). Expression of the surrogate light chains λ5 and VpreB was, however, not down-regulated in *Ikzf1* mutant Kit^{lo} cells in contrast to the large c-Kit^{lo} and small CD2^{+} pre-B cells of control mice (Fig. 2c), suggesting that pre-BCR signaling was defective despite expression of all pre-BCR components including the signaling chains Igα and Igβ (see below). As the *Ikzf1* mutant c-Kit^{lo} cells in the absence of pre-BCR signaling did not express pre-B cell-specific features other than Igμ expression, we refer to these cells as aberrant c-Kit^{lo} 'pro-B' cells. Notably, we could propagate the *Ikzf1* mutant pro-B cells in vitro in the presence of IL-7 and stromal OP9 cells, as they had only a minor cell cycle defect under these pro-B cell culture conditions (Supplementary Fig. 3a-e).

Half of the c-Kit^{hi} pro-B cells in *Cd79a*-Cre *Ikzf1*$^{fl/-}$ mice expressed the Igμ chain compared to only 15% of the c-Kit^{hi} pro-B cells of control *Cd79a*-Cre *Ikzf1*$^{fl/+}$ littermates (Fig. 2c), suggesting that Igμ expression provides a survival advantage in vivo in the absence of Ikaros. To test this idea, we analyzed the effect of *Ikzf1* inactivation on a Rag2-deficient background, which prevents V(D)J recombination at the *Igh* locus19. Indeed, pro-B cells in the bone marrow of *Cd79a*-Cre *Ikzf1*$^{fl/-}$ *Rag2*$^{-/-}$ mice were reduced 3-fold due to a preferential loss of c-Kit^{int} pro-B cells relative to control *Cd79a*-Cre *Ikzf1*$^{fl/+}$ *Rag2*$^{-/-}$ littermates (Supplementary Fig. 3f-h). Collectively, these data demonstrate that pro-B cell-specific inactivation of *Ikzf1* arrests development at an aberrant c-Kit^{lo} Igμ^{+} 'pro-B' cell stage due to a pre-BCR signaling defect.

Identification of regulated Ikaros target genes in pro-B cells

To determine the genome-wide binding pattern of Ikaros, we used short-term cultured pro-B cells from the bone marrow of *Ikzf1*$^{ihCd2/ihCd2}$ *Rosa26*$^{BirA/BirA}$ *Rag2*$^{-/-}$ mice and MACS-enriched CD4^{+}CD8^{+} double-positive (DP) thymocytes from *Ikzf1*$^{ihCd2/ihCd2}$ *Rosa26*$^{BirA/BirA}$ mice for streptavidin-mediated chromatin precipitation coupled with deep sequencing (Bio-ChIP-seq)20. Bio-ChIP-seq identified genes with unique Ikaros peaks in pro-B cells (*Nkd2*) or DP thymocytes (*Syt13*) as well as common Ikaros-binding sites in both cell types (*Malt1*; Fig. 3a,b). Peak calling with a stringent p-value of $< 10^{-10}$ determined 9,878 and 7,740 Ikaros-binding regions (Fig. 3b), which defined 8,391 and 4,989 Ikaros target genes with an overlap of 3,633 genes in pro-B and DP T-cells, respectively (Fig. 3c). By analyzing the sequences at Ikaros peaks with de novo motif discovery programs, we identified similar Ikaros-binding motifs in pro-B and DP T-cells (Fig. 3d),

which resemble published Ikaros consensus recognition sequences21,22. These Ikaros-binding motifs were found at a high frequency in common and unique Ikaros peaks of both cell types (Fig. 3d), thus confirming the specificity of Ikaros binding at the peaks identified by Bio-ChIP-seq.

To identify regulated Ikaros target genes, we analyzed Ikaros-deficient and control pro-B cells by RNA-sequencing. To this end, we isolated c-Kit^{hi} pro-B cells from the bone marrow of experimental *Cd79a*-Cre *Ikzf1*$^{fl/-}$ and control *Cd79a*-Cre *Ikzf1*$^{fl/+}$ mice by FACS sorting (Supplementary Fig. 4a) or cultured the respective pro-B cells for 5-7 days on stromal OP9 cells in the presence of IL-7 (Supplementary Fig. 3a). RNA-seq analysis revealed only exon 8-deleted *Ikzf1* transcripts in cultured *Cd79a*-Cre *Ikzf1*$^{fl/-}$ (*Ikzf1*$^{\Delta/-}$) pro-B cells in contrast to the presence of low levels of exon 8-containing mRNA in ex vivo sorted *Cd79a*-Cre *Ikzf1*$^{fl/-}$ pro-B cells (Supplementary Fig. 4b,c). Consequently, RNA transcripts of the activated Ikaros target gene *Cplx2* were more strongly reduced in cultured *Ikzf1*$^{\Delta/-}$ pro-B cells compared to ex vivo sorted *Ikzf1*$^{\Delta/-}$ pro-B cells (Fig. 3e). *Ramp1* was identified as a repressed Ikaros target gene, as its expression was induced in cultured and ex vivo sorted *Ikzf1*$^{\Delta/-}$ pro-B cells (Fig. 3e). As Ikaros-regulated genes were more strongly affected in cultured *Ikzf1*$^{\Delta/-}$ pro-B cells due to complete loss of the Ikaros protein (Supplementary Fig. 3c), we further analyzed the RNA-seq data of in vitro cultured pro-B cells by stringent filtering for > 3-fold gene expression changes. Activated and repressed genes were additionally selected for gene expression levels of > 5 RPKM in control *Ikzf1*$^{\Delta/+}$ pro-B cells (activated) or *Ikzf1*$^{\Delta/-}$ pro-B cells (repressed), respectively. Based on these stringent criteria, we identified 215 Ikaros-activated and 295 Ikaros-repressed genes in pro-B cells. When we additionally considered Ikaros binding at these regulated genes (100%), we identified 131 (60%) potentially directly activated and 180 (61%) potentially directly repressed Ikaros target genes (Supplementary Table 1), which are ranked according to their fold expression change in the bar plot of Fig. 3f and to their normalized expression values in the scatter plot of Fig. 3g. Scatter plot analysis of the RNA-seq data obtained with ex vivo sorted *Ikzf1*$^{\Delta/-}$ and *Ikzf1*$^{\Delta/+}$ pro-B cells (Fig. 3h) largely confirmed the repressed and activated target genes identified in cultured pro-B cells, although the fold expression change was lower for ex vivo sorted pro-B cells due to incomplete loss of *Ikzf1* expression.

Function of Ikaros target genes

The 131 activated and 180 repressed Ikaros target genes code for proteins of distinct functional classes (Fig. 4a; Supplementary Table 1). Intriguingly, the largest functional class of both activated and repressed Ikaros target genes encodes 31 (24%) and 39 (22%) signal transducers, respectively, indicating that Ikaros fulfills an important role in controlling intracellular signaling (Fig. 4a). Notably, the second largest functional class consists of 19 activated and 18 repressed cell surface receptor genes. By flow cytometric analysis of *Ikzf1* mutant and control pro-B cells, we could verify the activation of *Icam1* and *Bst1* as well as the repression of *Cd22* and *Cd72* at the protein level (Fig. 4b). Moreover, 13 activated and 19 repressed Ikaros target genes code for transcriptional regulators, which may be responsible for indirect effects of Ikaros-mediated gene control (Fig. 4a).

One of the repressed target gene, *Ikzf3*, codes for the transcription factor Aiolos, the most closely related family member of Ikaros23. *Ikzf3* expression was derepressed in cultured and ex vivo c-Kit^{hi} pro-B cells of *Cd79a*-Cre *Ikzf1*$^{fl/-}$ mice (Supplementary Fig. 4d,e). Single-cell analysis of intracellular Aiolos staining revealed that a large proportion of the in vitro and ex vivo *Ikzf1* mutant pro-B cells expressed the Aiolos protein at the same level as small pre-B cells of control mice (Fig. 4c). Hence, Aiolos cannot compensate for the loss of Ikaros in early B-cell development, indicating that Aiolos and Ikaros have non-redundant functions despite their high sequence similarity.

Ikaros controls intracellular signaling pathways of the pre-BCR

Consistent with Ikaros controlling the pro-to-pre-B cell transition, several Ikaros-activated genes code for positive regulators of (pre-)BCR signaling such as a costimulatory receptor (Slamf6), adaptor proteins (Lcp2 [SLP76], Lat, Grap2), kinases (Blk, PI3K subunit Pik3r5) and the phosphatase calcineurin (subunit Ppp3cc) (Fig. 4a and Supplementary Fig. 5a). Moreover, Ikaros represses genes coding for negative regulators of (pre-)BCR signaling including inhibitory receptors (Cd22, Cd72, Fcgr2b [FcγRIIb], Pdcd1 [PD1]) and phosphatases (Ptpn6 [SHP1], Inppl1 [SHIP2]) (Fig. 4a,b and Supplementary Fig. 5a). Hence, deregulation of these Ikaros target genes in Ikaros-deficient pro-B cells could explain the observed B-cell developmental block. To directly investigate intracellular signaling downstream of the pre-BCR, we took advantage of Igμ-negative *Rag2*$^{-/-}$ pro-B cells, which express the signaling chains Igα and Igβ in a complex with calnexin on their cell surface24. Crosslinking of this complex with the anti-Igβ antibody HM79 mimics pre-BCR signaling leading to pre-B cell development in vivo24. Anti-Igβ stimulation efficiently induced intracellular calcium mobilization in control *Cd79a*-Cre *Ikzf1*$^{fl/+}$ *Rag2*$^{-/-}$ pro-B cells in contrast to an anti-TCRγδ isotype control antibody (Fig. 5a). Intracellular calcium signaling was, however, not observed in *Cd79a*-Cre *Ikzf1*$^{fl/-}$ *Rag2*$^{-/-}$ pro-B cells upon Igβ crosslinking (Fig. 5a). Moreover, anti-Igβ stimulation was unable to induce phosphorylation of Akt (S473) in response to phosphoinositide 3-kinase (PI3K) activation in *Cd79a*-Cre *Ikzf1*$^{fl/-}$ *Rag2*$^{-/-}$ pro-B cells, although it increased p-Akt (S473) levels in control *Cd79a*-Cre *Ikzf1*$^{fl/+}$ *Rag2*$^{-/-}$ pro-B cells (Fig. 5b). Likewise, phosphorylation of Erk1/2 (T202/Y204) was not observed in the absence of Ikaros (Fig. 5b). Together, these data revealed an important role of Ikaros in activating the downstream PI3K, MAPK and calcium signaling pathways of the pre-BCR.

Ikaros regulates cell adhesion and migration

Ikaros activates genes coding for adhesion and chemokine receptors (Icam1 [CD54], Bst1 [CD157], Cxcr5), a Ras effector (Rassf5) and an adaptor molecule (Grb7) that have been implicated in cell adhesion and migration (Fig. 4a,b and Supplementary Fig. 5b). However, Ikaros primarily represses target genes coding for adhesion (Cdh22, Itga9, Plxnb2, Cd82), a chemokine receptor (Ccr2), kinases (Wnk2, Pkn3, Ptk2 [FAK1]), an adaptor molecule (Jub), a GTPase (Rhoq) and seven guanine nucleotide-exchange factors (Tiam2, Bcar3, Dock1, Dock6, Trio, Fgd1, Swap70), which induce signaling of the small GTPases Cdc42, Rac, and Rho leading to actin polymerization and cytoskeletal rearrangements (Fig. 4a and Supplementary Fig. 5b). These findings suggest that Ikaros controls the migration and adhesion behavior of pro-B cells. In a transwell migration assay, *Cd79a*-Cre *Ikzf1*$^{fl/-}$

Rag2$^{-/-}$ pro-B cells were unable to migrate towards a source of the chemokine CXCL12 (SDF-1α) in comparison to control *Cd79a*-Cre *Ikzf1*$^{fl/+}$ *Rag2*$^{-/-}$ pro-B cells (Fig. 5c), although *Cxcr4* encoding the CXCL12 receptor was similarly expressed in both cell types (data not shown). By contrast, the *Cd79a*-Cre *Ikzf1*$^{fl/-}$ *Rag2*$^{-/-}$ pro-B cells in the presence of CXCL12 adhered 6 times better than the control *Rag2*$^{-/-}$ pro-B cells to a surface coated with VCAM-1, the ligand for the integrin VLA-4 (Itga4/Itgb1) receptor, which was similarly expressed in the two pro-B cell types (data not shown). Hence, Ikaros promotes pro-B cell migration and simultaneously prevents cell adhesion in early B-lymphopoiesis.

Ikaros predominantly binds to active promoters and enhancers

To gain mechanistic insight into Ikaros-mediated gene regulation, we next investigated how Ikaros interacts with the regulatory landscape of *Rag2*$^{-/-}$ pro-B cells20 that we previously determined by genome-wide mapping of DNase I hypersensitive (DHS) sites and active *t*ranscription *s*tart *s*ites (TSS; identified by the *c*ap *a*nalysis of *g*ene *e*xpression [CAGE] method25). As shown in Fig. 6a, over half (5,348; 54%) of all Ikaros-binding sites were located at active promoters defined by the presence of active TSSs (CAGE reads). Moreover, one third (2,932; 30%) of all Ikaros peaks mapped to distal elements (DE), which are characterized by the presence of a DHS site in the absence of an active TSS (no significant CAGE reads). Subdivision of distal elements into active enhancers as well as poised, inactive and repressed distal elements by genome-wide mapping of active (H3K4me2, H3K4me3, H3K9ac) and repressive (H3K27me3) histone marks20 revealed that 71% (2,073) of all Ikaros-bound distal elements correspond to active enhancers (Fig. 6a). Moreover, by considering all regulatory elements of the pro-B cell genome, we could demonstrate that Ikaros bound to 60% of all active promoters in contrast to 12% of all inactive promoters (Fig. 6b). Ikaros binding was furthermore enriched at active enhancers (30%) compared to all distal elements (12%). We conclude therefore that Ikaros preferentially binds to active promoters and enhancers in pro-B cells.

As de novo motif discovery analysis of Ikaros-binding regions did not identify a significant recognition sequence for a transcription factor other than Ikaros, we determined the co-localization of Ikaros peaks with binding sites of Pax5, EBF1, PU.1 and IRF4 in pro-B cells by multiple overlap analysis of the corresponding ChIP-seq data20,26 (see Online Methods). Some Ikaros target genes with co-occurring binding sites for these transcription factors are shown in Supplementary Fig. 6a. As demonstrated in Fig. 6c, there was a high co-occurrence of IRF4 (73%)- and PU.1 (54%)-binding sites at all Ikaros peaks (9,878). Similar frequencies of co-localization were seen for IRF4- and PU.1-binding sites at Ikaros peaks of activated Ikaros target genes, whereas the reduced co-occurrence observed at repressed Ikaros target genes resulted in an increase of Ikaros-only peaks by 11%. In contrast, binding sites of the B-cell commitment factors EBF1 and Pax5 were present at a lower frequency at all Ikaros peaks, but were enriched at regulated Ikaros target genes. In particular, activated Ikaros target genes revealed an increased co-occurrence of binding sites for all three transcription factors (Fig. 6d). As regulated Pax5 target genes have been identified in pro-B cells20, we determined how many of the activated and repressed Ikaros target genes with co-occurrence of Ikaros- and Pax5-binding sites are also dependent on Pax5 for their expression in pro-B cells. Notably, Pax5 regulated 25% and 28% of these activated (99) and repressed

(100) Ikaros target genes, respectively (Supplementary Fig. 6b), which represents a significant enrichment compared to the 1.5% activated and 3% repressed Pax5 target genes identified among all Pax5-bound genes in pro-B cells20. Theses data therefore suggest that Ikaros cooperates with Pax5 to regulate some of its target genes.

Chromatin changes at promoters and enhancers of regulated Ikaros target genes

To investigate how Ikaros influences the chromatin state at promoters and enhancers of its target genes, we mapped, by ChIP-seq, the active histone marks H3K4me3 and H3K9ac in short-term cultured *Cd79a*-Cre *Ikzf1*$^{fl/-}$ *Rag2*$^{-/-}$ and *Cd79a*-Cre *Ikzf1*$^{fl/+}$ *Rag2*$^{-/-}$ pro-B cells. For analysis of these ChIP-seq data, we classified all genes according to their degree of Ikaros-dependent regulation and the presence or absence of Ikaros-binding sites at their regulatory elements. As shown by density diagrams (Fig. 7), the loss of Ikaros led to an increased abundance of the active histone marks H3K4me3 and H3K9ac at promoters and distal elements of the most strongly (> 5-fold) repressed Ikaros target genes, whereas it resulted in a significant reduction of the same histone modifications at promoters and enhancer of highly (> 5-fold) activated Ikaros target genes. Notably, indirectly Ikaros-regulated genes were characterized by a considerably lower density of H3K4me3 and H3K9ac at their promoter and distal elements lacking Ikaros binding (Fig. 7), although these genes were similarly expressed compared to the regulated Ikaros target genes (data not shown). Together, these data indicate a role for Ikaros in the induction or suppression of active chromatin at activated and repressed target genes, respectively.

As Ikaros has been implicated in chromatin regulation through its interaction with the nucleosome-remodeling and histone-deacetylase (NuRD) complex27,28, we mapped the NuRD component Mi-2β (CHD4) by ChIP-seq in short-term cultured *Cd79a*-Cre *Ikzf1*$^{fl/-}$ (*Ikzf1*$^{\Delta/-}$) and control *Cd79a*-Cre *Ikzf1*$^{fl/+}$ (*Ikzf1*$^{\Delta/+}$) pro-B cells by using a p-value of < 10^{-10} for peak calling. The 6,611 Mi-2β peaks identified at promoters in control *Ikzf1*$^{\Delta/+}$ pro-B cells revealed a large overlap (71%) with Ikaros peaks and a strong correlation between the binding density of the two transcription factors at promoters (Supplementary Fig. 7a,b), consistent with the notion that Ikaros can recruit the NuRD complex to its binding sites22,27. In contrast, there was little correlation between Mi-2β and Ikaros binding at distal element in pro-B cells, as Ikaros bound to only 26% of all Mi-2β peaks (11,987) at these elements (Supplementary Fig. 7a,b). Importantly, the binding of Mi-2β was similar in Ikaros-deficient (*Ikzf1*$^{\Delta/-}$) and control (*Ikzf1*$^{\Delta/+}$) pro-B cells (Supplementary Fig. 7b,c). Moreover, the loss of Ikaros did not affect the abundance of H3K9ac at Mi-2β- and Ikaros-binding sites in pro-B cells (Supplementary Fig. 7b,c) in contrast to the observed global decrease of H3K9 acetylation at the corresponding sites in *Ikzf1*$^{-/-}$ thymocytes22. Together, our data do not support a role for the NuRD complex in controlling the observed chromatin changes at promoters and distal elements of the regulated Ikaros target genes in early B cell development.

Ikaros regulates distinct target genes during early B-lymphopoiesis

As Ikaros is similarly expressed in lymphoid progenitors, pro-B and pre-B cells (Fig. 1a), we investigated by RNA-seq how the regulated Ikaros target genes identified in pro-B cells (Fig. 3f,g) are expressed during the transition from B-cell-biased lymphoid progenitors (BLPs) to

small pre-B cells. As shown in Fig. 8a, the Ikaros target genes *Pld4*, *Cenpv* and *Emid1* were repressed in pro-B cells, while being expressed in BLPs and pre-B cells. A similar trend was also seen for repressed Ikaros target genes involved in cell migration and adhesion (Supplementary Fig. 8a). Conversely, the target genes *Nkd2*, *Alpl* and *Smtnl2* were activated in pro-B cells, but repressed in BLPs and pre-B cells (Fig. 8a). To examine whether these findings can be generalized, we highlighted all activated (blue) and repressed (red) Ikaros target genes (identified in pro-B cells) in the scatter plots displaying the gene expression differences from BLPs to pro-B cells and from pro-B to pre-B cells (Fig. 8b). Moreover, we plotted the fold expression change of the regulated Ikaros target genes for each cell pair as a density diagram (Fig. 8c). As shown by these analyses, most repressed Ikaros target genes in pro-B cells were up-regulated in BLPs and pre-B cells, whereas the majority of activated Ikaros target genes were highly expressed only in pro-B cells. These data therefore suggest that Ikaros target genes are differentially regulated at the onset of B-cell development.

The dynamic regulation of Ikaros target genes may reflect differential binding of Ikaros in early B-lymphopoiesis, which we investigated by Bio-ChIP-sequencing of cultured *Vav*-Cre *Ebf1*$^{fl/fl}$ (*Ebf1*$^{\Delta/\Delta}$) *Ikzf1*$^{ihCd2/ihCd2}$ *Rosa26*$^{BirA/+}$ pre-pro-B cells. Comparison of the Ikaros binding pattern between *Ebf1*$^{\Delta/\Delta}$ pre-pro-B and *Rag2*$^{-/-}$ pro-B cells revealed 4455 common Ikaros peaks, whereas more than half of all Ikaros peaks were preferentially bound in only one of the cell types (Fig. 8d). To identify regulated Ikaros target genes in pre-pro-B cells, we used a tetracycline-inducible shRNA expression system29 with the improved miR-E backbone30 to down-regulate Ikaros function in *Ebf1*$^{-/-}$ pre-pro-B cells. We infected *Ebf1*$^{-/-}$ pre-pro-B cells with the TRMPVIR retrovirus29 containing two independent *Ikzf1* shRNAs (Ik4056 or Ik2709) or a control shRNA (Ren713) targeting *Renilla* luciferase (Supplementary Fig. 8b-e), and sorted infected Venus^{+}dsRed^{+} cells after 4 days of doxycycline-induced shRNA expression. RNA-seq comparison between Ik4056 shRNA-expressing and control pre-pro-B cells identified 73 Ikaros-activated and 193 Ikaros-repressed genes (with an adjusted p-value of < 0.1; Fig. 8e), which were largely confirmed by RNA-seq analysis of pre-pro-B cells expressing the less efficient Ik2709 shRNA (Supplementary Fig. 8e,f). Ikaros bound to a subset of these regulated genes in pre-pro-B cells (Fig. 8f). Importantly, the majority of the regulated Ikaros target genes, which were identified in pro-B cells (Fig. 3f,g) and futher implicated in pre-BCR signaling or cell migration/adhesion (Supplementary Fig. 5a,b), were not regulated by Ikaros in pre-pro-B cells (Fig. 8g,h). Together these data demonstrate that Ikaros binds to and regulates distinct target genes at different stages of early B-cell development.

Discussion

Ikaros is an essential regulator of early B-cell development2,6,7. Here, we have demonstrated that the loss of Ikaros in pro-B cells arrested B-cell development at a small aberrant c-Kit^{lo} ‘pro-B’ cell stage due to a pre-BCR signaling defect. Using ChIP- and RNA-seq approaches, we identified a plethora of activated and repressed Ikaros target genes, which provided insight into the molecular function of Ikaros in early B-lymphopoiesis.

The expression of Aiolos, a closely related family member of Ikaros23, is strongly activated upon pre-BCR signaling10. In contrast to the loss of Ikaros, Aiolos deficiency results in a 2-

fold increase of large and small pre-B cells in *Ikzf3*$^{-/-}$ mice31,32. Here, we identified *Ikzf3* (Aiolos) as a repressed Ikaros target gene, which suggests that its Ikaros-mediated repression must be antagonized by pre-BCR signaling possibly through the combined action of IRF4 and IRF8 (ref. 11) or posttranslational modifications33. Derepression of Aiolos could, however, not compensate for the loss of Ikaros, as it failed to rescue the developmental block of Ikaros-deficient pro-B cells. Hence, Aiolos and Ikaros must have non-redundant functions in pre-BCR signaling at least with regard to the regulation of a subset of their target genes.

Although Ikaros is similarly expressed throughout early B-cell development, its activated and repressed target genes identified in pro-B cells were differently regulated earlier in lymphoid progenitors (BLPs, pre-pro-B cells) and later in small pre-B cells. This dynamic expression pattern could be explained by the observed stage-specific binding of Ikaros as well as by the cooperation of Ikaros with different transcription factors at its target genes. The latter point is best exemplified by the B-lineage commitment factor Pax5, which is absent in lymphoid progenitors but is expressed in pro-B cells34, where its binding was enriched at Ikaros peaks of activated Ikaros target genes. The observed minimal overlap of Ikaros-regulated genes between pre-pro-B and pro-B cells provided further evidence that Ikaros regulates its target genes in a stage-specific manner similar to Pax5 and EBF1 in early and late B-cell development20,26.

The stringent block at the pro-B-to-pre-B cell transition in *Cd79a*-Cre *Ikzf1*$^{fl/-}$ mice is caused by a strong defect of pre-BCR signaling. Although Ikaros-deficient pro-B cells expressed all components of the pre-BCR, they were unable to activate the PI3K, MAPK and calcium signaling pathways upon pre-BCR stimulation. This phenotype is nicely explained by the dual role of Ikaros in activating genes coding for positive regulators of these downstream signaling pathways including adaptor proteins (SLP76, LAT, Grap2), kinases (PI3K subunits, BLK) and calcineurin (Ppp3cc), while simultaneously repressing genes coding for negative regulators of pre-BCR signaling such as inhibitory receptors (CD22, CD72, FcγRIIb, PD1) and phosphatases (SHP1, SHIP2). Notably, the increased expression of these inhibitory receptors and their associated protein phosphatase SHP1 in Ikaros-deficient pro-B cells may interfere with signaling of all downstream pre-BCR pathways by antagonizing phosphorylation of the Syk kinase9.

The increased substrate adhesion and reduced migration of Ikaros-deficient pro-B cells identified a novel function of Ikaros in early B-cell development. Cells adhere to the extracellular matrix primarily via integrin-linked focal adhesion complexes, which induce, in response to integrin clustering, signaling via the focal adhesion kinase (FAK1, Ptk2) to the small GTPases Rho, Rac and Cdc42, leading to actin cytoskeletal rearrangements. While activating 5 genes in pro-B cells, Ikaros repressed 17 genes with known functions in cell adhesion and migration including adhesion molecules (Cdh22, Itga9, Plxnb2, Cd82), kinases (Wnk2, Pkn3, Ptk2 [FAK1]) and guanine nucleotide-exchange factors (Tiam2, Bcar3, Dock1, Dock6, Trio, Fgd1, Swap70), which activate, with different specificities, the small GTPases Rho (Trio)35, Rac (Tiam2, Dock1, Swap70)36–38 and Cdc42 (Dock6, Fdg1, Bcar3)39–41. The increased expression of FAK1 and the 7 guanine nucleotide-exchange factors likely contributes to the efficient substrate adhesion of Ikaros-deficient pro-B cells by enhancing the activity of multiple small GTPases. Cell adhesion and migration is

dynamically regulated during early B-cell development, as uncommitted pre-pro-B cells adhere to CXCL12-expressing reticular cells and pro-B cells to IL-7-expressing stromal cells, while pre-B cells migrate away from both bone marrow niches42. Notably, the 'adhesion/migration' genes, which are repressed by Ikaros in pro-B cells, are highly expressed in BLPs and/or pre-B cells, indicating that Ikaros contributes to the dynamic regulation of cell adhesion and migration during early B-cell development.

We furthermore demonstrated a role for Ikaros in inducing active chromatin at promoters and enhancers of activated target genes and in chromatin silencing at regulatory elements of repressed target genes. Ikaros has been implicated in chromatin regulation through its interaction with the nucleosome-remodeling and histone-deacetylase (NuRD) complex27,28. As DNA-binding component, Ikaros tethers the Mi-2β-containing NuRD complex to permissive chromatin of active genes in double-positive T-cells22. Notably, Ikaros binding seems to negatively regulate the activity of the NuRD complex, as its loss leads to a local increase in chromatin remodeling and histone deactylation22. Like in *Ikzf1* mutant T-cells22, the NuRD complex remained bound at Ikaros-binding sites in Ikaros-deficient pro-B cells. In analogy to the T cell situation22, increased NuRD activity in the absence of Ikaros could be responsible for the loss of H3K9ac at regulatory elements of activated Ikaros target genes, but fails to explain the observed increase of H3K9ac at repressed target genes in Ikaros-deficient pro-B cells. In contrast to the *Ikzf1* mutant T-cells22, we did not observe a global reduction of H3K9 acetylation at Mi-2β- and Ikaros-binding sites in Ikaros-deficient pro-B cells, which may indicate a different role of Ikaros in chromatin regulation during early B and T cell development. Alternatively, the discrepancy could be caused by the different deletion strategies used, as the H3K9ac pattern may never be properly established in the absence of Ikaros during the differentiation of HSCs to thymocytes in *Ikzf1*$^{-/-}$ mice, whereas our conditional mutagenesis acutely inactivated *Ikzf1* only at the pro-B cell stage. Notably, Ikaros also interacts with the co-repressor CtBP43 and HDAC-containing Sin3 complexes44, both of which may be involved in chromatin silencing at repressed Ikaros target genes. These interpretations are, however, complicated by the fact that Aiolos not only interacts with the NuRD and Sin3 co-repressor complexes like Ikaros44,45, but is also expressed in *Ikzf1* mutant pro-B cells. The observed chromatin changes in Ikaros-deficient pro-B cells may therefore suggest that Ikaros and Aiolos also have some non-redundant functions in chromatin regulation.

The *IKZF1* gene is a potent tumor suppressor gene in BCR-ABL1-positive B-ALL3. Over half of the *IKZF1* mutations in B-ALL are heterozygous focal deletions eliminating exons 4-7, thus resulting in expression of the dominant-negative isoform IK6 (ref. 3,46). Notably, homozygous deletions of the entire *IKZF1* gene are observed in 11-14% of all B-ALL cases with *IKZF1* mutations3,46. Hence, the deregulation of gene expression, identified upon Ikaros loss in this study, may also contribute to the formation of B-ALL, which is arrested at an early stage similar to B-cell development in *Cd79a*-Cre *Ikzf1*$^{fl/-}$ mice. Surprisingly however, *Cd79a*-Cre *Ikzf1*$^{fl/-}$ mice did not develop B-cell leukemia despite accumulation an aberrant 'pro-B' cell population. Hence, similar to *PAX5* mutations47, the loss of Ikaros contributes to B-ALL development only in the presence of additional driver mutations, which will be an interesting topic for future studies.

Online Methods

Mice

The following mice were maintained on the C57BL/6 genetic background: *Ikzf1*$^{+/-}$ (ref. 1), *Ebf1*$^{+/-}$ (ref. 2), *Ebf1*$^{fl/fl}$ (ref. 3), *Rosa26*$^{BirA/BirA}$ (ref. 4), *Rag2*$^{-/-}$ (ref. 5), *Cd79a*$^{Cre/+}$ (ref. 6), *Mox2*$^{Cre/+}$ (ref. 7), *Il7r*$^{Cre/+}$ (ref. 8), transgenic *Vav*-Cre (ref. 9) and transgenic FLPe mice10. Throughout the manuscript, the heterozygous *Cd79a*$^{Cre/+}$ genotype is referred to as *Cd79a*-Cre. All animal experiments were carried out according to valid project licenses, which were approved and regularly controlled by the Austrian Veterinary Authorities.

Generation of the *Ikzf1*^{ihCd2} allele

The targeting vector for generating the *Ikzf1*^{ihCd2} allele was obtained by first inserting the following sequences in the 5' to 3' direction (Supplementary Fig. 1a) into the *Ikzf1* BAC bMQ-185J16 (129Sv) by recombineering in *E. coli*; a 233-bp MfeI-AscI fragment containing C-terminal tag sequences (fused in frame to the last *Ikzf1* codon), a 1.8-kb AscI-SalI fragment containing the IRES-*hCd2* (ihCd2) reporter gene (flanked by *frt* sites) and a 1.9-kb SalI-XhoI fragment containing the mouse phosphoglycerate kinase (PGK) promoter linked to the neomycin (Neo) resistance gene (flanked by *loxP* sites). The tag sequences contained cleavage sites for the PreScission (PreSc) and TEV proteases, epitopes for Flag and V5 antibodies and a biotin acceptor sequence (Biotin) for biotinylation by the *Escherichia coli* biotin ligase BirA11. In a second step, the *Ikzf1*^{ihCd2} targeting vector was generated by excising and inserting the integrated sequences together with the flanking 5' (5.0 kb) and 3' (1.7 kb) homology regions by recombineering from the modified BAC into the pBV-DTA-pA plasmid containing an *HSV-TK* gene (for negative selection). SgrA1-linearized DNA (15 μg) was electroporated into cells ($1x10^7$) of the hybrid C57BL/6 x 129Sv ES cell line A9 followed by selection with 250 μg/ml G418. PCR-positive clones were verified by Southern blot analysis prior to injection into C57BL/6 blastocysts and the generation of *Ikzf1*$^{ihCd2\text{-}Neo/+}$ mice. The *Ikzf1*^{ihCd2} allele was obtained by crossing *Ikzf1*$^{ihCd2\text{-}Neo/+}$ mice with *Mox2*$^{Cre/+}$ mice7 and was verified by Southern blot analysis of XbaI-digested tail DNA. The following primers were used for PCR genotyping of *Ikzf1*$^{hCd2/+}$ mice: (a) 5'-GAGGAGTCGGAGAAATGATGAG-3'; (b) 5'-TCCACAGATACAGAGAGCAACG-3'; (c) 5'-GGAGAGTGTTAGGAAGCCACAT-3'. The *Ikzf1*^{ihCd2} allele was identified as an 834-bp PCR fragment with the primer pair a/c and the wild-type *Ikzf1* allele as 645-bp PCR fragment with the primer pair b/c (Supplementary Fig. 1b).

Generation of the floxed *Ikzf1* allele

The conditional *Ikzf1* targeting vector was assembled in the pBV-DTA-pA plasmid containing an *HSV-TK* gene (for negative selection) as well as a polylinker with appropriate restriction sites for insertion of the following sequences in the 5' to 3' direction (Supplementary Fig. 2a); a 4.8-kb NotI-SfiI fragment (cloned as long 5' homology region from the *Ikzf1* BAC bMQ-185J16 by recombineering in *E. coli*), a 5' *loxP* site present in the polylinker, a 3.5-kb SalI-AscI fragment (containing the entire *Ikzf1* exon 8 including the 3' untranslated sequences), a 1.3-kb SacII-SalI fragment (containing 6 copies of the SV40 polyA region and the 3' *loxP* site), a 2.2-kb ClaI-MluI fragment (containing the PGK-Neo

resistance gene flanked by *frt* sites) and a 1.9-kb XmaI-BsiWI fragment (cloned as short 3' homology region from the same *Ikzf1* BAC by recombineering). PvuI-linearized DNA (15 μg) was electroporated into cells ($1x10^7$) of the hybrid C57BL/6 x 129Sv ES cell line A9 followed by selection with 250 μg/ml G418. PCR-positive clones were injected into C57BL/6 blastocysts to generate $Ikzf1^{fl\text{-}neo/+}$ mice. The $Ikzf1^{fl}$ allele was obtained by crossing $Ikzf1^{fl\text{-}neo/+}$ mice with the FLPe line10, and both alleles were verified by Southern blot analysis of KpnI-digested tail DNA (Supplementary Fig. 2b). The following primers flanking the 5' *loxP* site were used for PCR genotyping of *Ikzf1* mutant mice: (a) 5'-TCCTGCTTCCTGTTTCTGCT-3'; (b) 5'-CAGGGGTTGAATGGTGTTCT-3'; (c) 5'-ACATGGTCCTGCTGGAGTTC-3'. The wild-type *Ikzf1* allele was identified as a 558-bp PCR fragment and the floxed $Ikzf1^{fl}$ allele as a 381-bp PCR fragment with the primer pair a/b (Supplementary Fig. 2c). The deleted $Ikzf1^{\Delta}$ allele was detected as a 484-bp PCR fragment with the primer pair a/c (Fig. 1d).

FACS analysis and sorting

The following antibodies were used for flow cytometric analysis: anti-Aiolos (8B2), B220/CD45R (RA3-6B2), BP-1 (6C3), CD2 (RM2-5), CD3ε (145-2C11), CD4 (GK1.5), CD8a (53-6.7), CD5 (53-7.3), CD11b/Mac1 (M1/70), CD11c (HL3, N418), CD16/32 (2.4G2), CD19 (1D3), CD21/CD35 (7G6), CD22 (Cy34.1), CD23 (B3B4), CD24/HSA (M1/69), CD25/IL-2Rα (PC61), CD28 (37.51), CD38 (90), CD40 (3/23), CD43 (S7), CD44 (IM781), CD49b (DX5), CD54 (YN1/1.7.4), CD55 (RIKO-5), CD72 (K10.6), CD79b (HM79), CD86 (GL1), CD93/AA4.1 (PB493), CD115/MCSF-R (AFS98), CD117/c-Kit (2B8), CD127/IL-7Rα (A7R34), CD135/Flt3 (A2F10.1), CD138 (281-2), CD179a/VpreB (R3), CD179b/λ5 (LM34), CD352 (13G3), F4/80 (CI:A3-1), Gr1 (RB6-8C5), MHCII (M5-114), IgD (11.26c), IgM (II/41), IgM^b (AF6-78), Ikaros (2A9), NK1.1 (PK136), Ly5.1 (A20), Ly5.2 (104), Ly6C (6C3), Ly6D (49H4), pAkt (S473, D9E), pErk1/2 (T202/Y204, 20A), Sca1/Ly6A (D7), TCRβ (H57-597), Ter119 (TER119), Thy1.2 (53-2.1) and human CD2 (RPA-2.10) antibodies. All cell type and expression analyses were performed with age-matched experimental and control mice and were repeated at least three times in independent experiments. Prism software (GraphPad) was used for statistical analysis.

FACS sorting and definition of hematopoietic cell types

The different hematopoietic cell types were identified by flow cytometry or sorted with a FACS Aria machine (Becton Dickinson) as follows: MPPs (LSKs; $Lin^-IL\text{-}7R\alpha^-Flt3^-Sca1^{hi}c\text{-}Kit^{hi}$), LMPPs ($Lin^-IL\text{-}7R\alpha^-Flt3^+Sca1^{hi}c\text{-}Kit^{hi}$), CLPs ($Lin^-IL\text{-}7R\alpha^+Flt3^+Sca1^{lo}c\text{-}Kit^{lo}$), ALP ($Ly6D^-$ CLPs), BLP ($Ly6D^+$ CLPs), pro-B ($CD19^+c\text{-}Kit^+CD25^-$[or $CD2^-$]IgM^-IgD^-), pre-B ($CD19^+CD25^+$[or $CD2^+$]$c\text{-}Kit^-IgM^-IgD^-$), immature B ($CD19^+IgM^{hi}IgD^{lo}$), mature B ($CD19^+$ IgM^{lo} IgD^{hi}), MZ B ($CD19^+CD21^{hi}CD23^{lo/-}$), FO B ($CD19^+CD21^{int}CD23^{hi}$), GC B ($CD19^+PNA^+Fas^+$), B-1 cells ($CD19^+B220^{lo/-}$), plasma cells ($Lin^-CD138^{hi}CD28^+$), total B cells ($CD19^+B220^+$), granulocytes ($Gr1^{hi}Mac1^{hi}$), erythroblasts ($c\text{-}Kit^+Ter119^+$), erythrocytes ($c\text{-}Kit^-Ter119^+$), macrophages ($Mac1^+MCSF\text{-}R^+$) as well as DN1 ($CD44^+CD25^-Thy1.2^+CD4^-CD8^-$), DN2 ($CD44^+CD25^+Thy1.2^+CD4^-CD8^-$), DN3 ($CD44^-CD25^+Thy1.2^+CD4^-CD8^-$), DN4 ($CD44^-CD25^-Thy1.2^+CD4^-CD8^-$), DP ($CD4^+CD8^+$) CD4 SP ($CD4^+CD8^-$) and CD8 SP ($CD4^-CD8^+$) thymocytes. Lineage-positive cells (Lin^+) cells were MACS-depleted and furthermore electronically gated away

with the following lineage (Lin) marker antibodies: B220, CD19, CD4, CD8a, TCRβ, DX5, Gr1, Ly6C, Mac1, CD11c, Ter119 (for MPPs, LMPPs, CLPs, ALPs and BLPs) and CD4, CD8a, CD21, F4/80 (for plasma cells).

In vitro culture of lymphoid progenitors

Cd79a-Cre *Ikzf1*$^{fl/-}$, *Cd79a*-Cre *Ikzf1*$^{fl/+}$ and *Rag2*$^{-/-}$ pro-B cells were cultured on OP9 cells in IL-7 containing IMDM as described12. EBF1-deficient progenitors were generated by in vitro culturing of sorted Lin^{-} bone marrow cells from *Ebf1*$^{-/-}$ mice in IL-7, Flt3L and SCF containing IMDM as described13.

Cell cycle analysis

Following intraperitoneal injection of BrdU (1 mg per mouse) for 40 min, bone marrow single-cell suspensions were prepared and stained for cell surface proteins (CD19, IgM, IgD, CD2, c-Kit). Cultured pro-B cells were treated with 10 μM BrdU for 30 or 45 min. BrdU stainings were performed with the BrdU flow kit (BD Bioscience) according to the manufacturer's protocol. Shortly, surface stained cells were fixed, permeabilized and DNase I-treated. Incorporated BrdU was stained with an anti-BrdU antibody and total DNA with 7-AAD. Single-cell analysis was performed on a Fortessa flow cytometer and evaluated by using the Flow-Jo software.

Calcium fluorimetry

Pro-B cells ($1x10^6$) were loaded with the calcium sensor dye eFluor 514 (eBioscience) at a final concentration of 1 μM in 1 ml of pro-B cell medium. After incubation at 37°C for 30 min, the cells were washed and the fluorescent emission at 530/30 nm (excitation at 488 nm) was measured in live cells on a Fortessa flow cytometer. The acquisition of the data was initiated 60 sec prior to the addition of the monoclonal anti-Igβ antibody HM79 (at 10 μg/ml). The data were collected for 300 sec and analyzed using the FlowJo software. The percentage of fluorescent increase ($\Delta F/F_0$) is plotted against time (t) after stimulation. F_0 refers to the average fluorescence determined between 0 and 30 sec prior to antibody addition, and ΔF corresponds to the measured fluorescence F(t) minus F_0.

Transwell migration assay

Pro-B cells were washed and resuspended at $3\text{-}5x10^6$ cells/ml in IMDM medium supplemented with 0.25% heat-inactivated fetal calf serum, 1 mM glutamine, 50 μM β-mercaptoethanol and 1% conditioned supernatant of rIL-7 producing J558L cells. The pro-B cell suspension (100 μl) was placed in the upper compartment and IL-7 medium (600 μl) containing 400 ng/ml CXCL12 (SDF-1α; Sigma) in the lower compartment of a transwell chamber (5 μm pore size; Corning Inc.). Pro-B cells migrating into the lower chamber were measured after 2 hours using a Casy cell counter, and their percentage relative to the total cells was calculated.

Adhesion assay

The adhesion of pro-B cells to VCAM1-coated chamber slide was analyzed as follows. Eight-well chamber slides (Nunc) were coated with recombinant mouse VCAM1-Fc protein

(25 mg/ml; R&D Systems) for 1.5 hour at room temperature, washed 3 time with PBS, before $1x10^5$ pro-B cells were added in 0.2 ml pro-B cells medium supplemented with 100 ng/ml CXCL12 (SDF-1α; Sigma). After incubation for 6 hours at 37°C, the chambers were removed, and the slides were washed with pre-warmed pro-B cell medium and then with PBS followed by fixation with 4% paraformaldehyde in PBS for 15 minutes at room temperature. The slides were washed 3 times with PBS, stained with 0.1% Crystal Violet for 30 min prior to washing with distilled water and drying. The number of cells that were attached to the glass slides was manually counted under the microscope. For each genotypes, the cells from 8 wells (0.7 cm^2) were counted to determine the cell number per cm^2.

Antibodies

The following antibodies were used for immunoblot analysis: anti-Ikaros (mouse mAb clone 4E9; from K. Georgopoulos, Harvard University), anti-TBP (mouse mAb clone 3TF1-3G3; Active Motif) and for cell stimulation or intracellular staining: anti-Igβ (Armenian hamster IgG2 mAb clone HM79; from Hajime Karasuyama, Tokyo), anti-TCRγδ (Armenian hamster IgG2 mAb clone GL-3), anti-pAkt (S473, D9E; Cell Signaling Technology), anti-pErk1/2 (T202/Y204, 20A; BD Bioscience), anti-Aiolos (8B2; eBioscience), anti-Ikaros (2A9, Biolegend; Supplementary Fig. 1f,g) and the rabbit polyclonal anti-Ikaros antibody (5443; Cell Signaling; Supplementary Fig. 8d,e).

Ikzf1 shRNA knock-down experiments

Two Ikaros-specific shRNA (Ik2709 and Ik4056) and control shRNA (Ren713) sequences were cloned as into the TRMPVIR vector14 containing the optimized miR-E backbone15. The following 22nt-shRNA guide sequences were used for cloning: 5'-TTTGTGGAATAACAGGTCCTGG-3' (Ik2709); 5'-TTAATCTCTGAATACCACTGGT-3' (Ik4056) and 5'-TAGATAAGCATTATAATTCCTA-3'(Ren713). Retroviruses was produced by transfecting 20 μg of the retroviral vector together with 10 μg of the helper vector into Plat-E packaging cells using standard calcium phosphate transfection in the presence of 25 μM chloroquine. Twenty-four hours after the transfection, the high-titer viral supernatant was collected in progenitor cell medium (IL-7, Flt3L and SCF containing IMDM)13, passed through a 0.45-μm filter and supplemented with 4 μg/ml of polybrene. The infection was carried out in a 6-well plate by spinning for 15 min. Each well contained $1x10^6$ *Ebf1*$^{-/-}$ progenitor cells with OP9 cells in progenitor cell medium containing 1 ml of freshly collected viral supernatant. Infection was repeated 5 times every 5-8 hours. Forty-eight hours after the last infection, the cells were treated with doxycycline (1 μg/ml) to induce shRNA expression. After 4 days of induction, GFP^{hi} dsRed^{hi} CD11b^{-} progenitor cells were FACS-sorted to select for high shRNA expression and against the presence of CD11b^{-} myeloid cells. The sorted cells were subjected to RNA preparation and cDNA synthesis followed by Illumina deep sequencing. For analysis of Ikaros protein expression, the doxycycline treatment was carried out for 3 days prior to intracellular FACS staining and immunoblotting of lysates prepared from FACS-sorted dsRed^{hi} cells.

ChIP-seq analysis of histone modifications and IRF4 and Mi-2β binding

Pro-B cells from the bone marrow of *Rag2*$^{-/-}$ mice were expanded in vitro for 4-5 days on OP9 cells in the presence of IL-7 prior to chromatin immunoprecipitation (ChIP) with an

anti-IRF4 antibody (goat polyconal antibody sc-6059; from Santa Cruz), as described in detail16. For chromatin profiling, pro-B cells from the bone marrow of *Cd79a*-Cre *Ikzf1*$^{fl/-}$ *Rag2*$^{-/-}$ and *Cd79a*-Cre *Ikzf1*$^{fl/+}$ *Rag2*$^{-/-}$ mice were short-term cultured as described above, and live pro-B cells were enriched by density gradient purification using Lympholyte M (Cedarlane Laboratories) prior to ChIP analysis16 with histone modification-specific antibodies. Rabbit polyclonal antibodies recognizing the following histone tail modifications were used for ChIP analysis: H3K4me3 (pAb-003-050) from Diagenode and H3K9ac (07-352) from Millipore. The ChIP efficiency was quantified by real-time PCR analysis with SYBR green as described13. The ChIP-precipitated DNA was submitted to Illumina deep sequencing.

For Mi-2β (CHD4) binding analysis, pro-B cells from the bone marrow of *Cd79a*-Cre *Ikzf1*$^{fl/-}$ and *Cd79a*-Cre *Ikzf1*$^{fl/+}$ mice were cultured as described above. Cells were then fixed with 2 mM DSG (disuccinimidyl glutarate; Sigma) for 45 min at room temperature prior to fixation with 1% formaldehyde for 10 min. The fixed cells were subjected to nuclei preparation and lysis, and the chromatin was sheered using a Biorupter™ sonicator (Diagenode) in the presence of 0.1% SDS. Immunoprecipitation was carried out with a mouse mAb against Mi-2β (3F2/4; Abcam) as described above. See Supplementary Table 2 for further information.

Bio-ChIP-seq analysis of Ikaros and PU.1 binding

Pro-B cells isolated from the bone marrow of *Ikzf1*$^{ihCd2/ihCd2}$ *Rosa26*$^{BirA/BirA}$ *Rag2*$^{-/-}$ or *Spi1*$^{ihCd2/ihCd2}$ *Rosa26*$^{BirA/BirA}$ mice were expanded in vitro for 4-6 days on OP9 cells in the presence of IL-7. *Ebf1*$^{\Delta/\Delta}$ pre-pro-B cells were generated by in vitro culturing of sorted Lin$^-$ bone marrow cells from *Vav*-Cre *Ebf1*$^{fl/fl}$ (*Ebf1*$^{\Delta/\Delta}$) *Ikzf1*$^{ihCd2/ihCd2}$ *Rosa26*$^{BirA/+}$ mice on OP9 cells in the presence of IL-7, SCF and Flt3L. Moreover, CD4$^+$CD8$^+$ double-positive (DP) thymocytes were enriched by CD8 MACS sorting from the thymus of *Ikzf1*$^{ihCd2/ihCd2}$ *Rosa26*$^{BirA/BirA}$ mice. Chromatin from ~1x10^8 pro-B cells or DP thymocytes was prepared using a lysis buffer containing 0.25% SDS (for Ikaros) or 1% SDS (for PU.1) prior to chromatin precipitation by streptavidin pulldown (Bio-ChIP), as recently described17. The precipitated genomic DNA was quantified by real-time PCR, and about 5 ng of ChIP-precipitated DNA was submitted to Illumina deep sequencing. See Supplementary Table 2 for further information.

cDNA preparation for RNA-sequencing

Pro-B cells from the bone marrow of *Cd79a*-Cre *Ikzf1*$^{fl/-}$, *Cd79a*-Cre *Ikzf1*$^{fl/+}$, *Cd79a*-Cre *Ikzf1*$^{fl/-}$ *Rag2*$^{-/-}$ and *Cd79a*-Cre *Ikzf1*$^{fl/+}$ *Rag2*$^{-/-}$ mice were cultured for 5-13 days on OP9 cells in IL-7 containing IMDM prior to FACS sorting of the pro-B cells (c-Kit^{hi}CD19$^+$CD2$^-$ CD5$^-$ IgM$^-$IgD$^-$). *Ebf1*$^{-/-}$ pre-pro-B cells, which were infected with different shRNA viruses and treated with doxycycline, were cultured in progenitor cell medium (IL-7, Flt3L and SCF containing IMDM)13. The following cell types were isolated ex vivo by FACS sorting: c-Kit^{hi} pro-B cells (c-Kit^{hi}CD19$^+$CD2$^-$IgM$^-$IgD$^-$) from *Cd79a*-Cre *Ikzf1*$^{fl/-}$ and *Cd79a*-Cre *Ikzf1*$^{fl/+}$ mice (Supplementary Fig. 4a) as well as wild-type pre-B cells (c-Kit$^-$ CD19$^+$CD2$^+$IgM$^-$IgD$^-$) containing > 90% small and <10% large pre-B cells.

RNA from these in vitro cultured and ex vivo sorted cells was isolated with the RNeasy Plus Mini Kit (Qiagen), and mRNA was obtained by two rounds of poly(A) selection using the Dynabeads mRNA purification kit (Invitrogen) followed by fragmentation by heating at 94°C for 3 min (in fragmentation buffer). The fragmented mRNA was used as template for first-strand cDNA synthesis with random hexamers using the Superscript III First-Strand Synthesis System (Invitrogen). The second-strand cDNA was synthesized with 100 mM dATP, dCTP, dGTP and dUTP in the presence of RNase H, *E. coli* DNA polymerase I and DNA ligase (Invitrogen). The incorporation of dUTP allowed elimination of the second strand during library preparation (see below), thereby preserving strand specificity18. See Supplementary Table 2 for further information.

Illumina deep sequencing

About 2-5 ng of cDNA or ChIP-precipitated DNA were used as starting material for the generation of single-end sequencing libraries as described by Illumina's ChIP Sequencing sample preparation protocol. DNA fragments of the following sizes were selected for the different experiments: 200–350 bp for ChIP-seq and 150–700 bp for RNA-seq. For strand-specific RNA-sequencing, the uridines present in one cDNA strand were digested with uracil-N-glycosylase (New England Biolabs) as described18 followed by PCR amplification. Completed libraries were quantified with the Agilent Bioanalyzer dsDNA 1000 assay kit and Agilent QPCR NGS library quantification kit. Cluster generation and sequencing was carried out by using the Illumina HiSeq 2000 system with a read length of 50 nucleotides according to the manufacturer's guidelines. Further information about all sequencing experiments generated for this study is presented in Supplementary Table 2.

Peak calling of ChIP-seq data and target gene assignment

Peaks were called using the MACS program version 1.3.6.1 (ref. 19) with default parameters, a read length of 36 nucleotides for ChIP-seq, a genome size of 2,654,911,517 bp (mm9) and the appropriate input control sample. Peaks were filtered for p-values of $< 10^{-10}$. This stringent cutoff efficiently removed false positive (unique) peaks of technical replicas. Ikaros peaks were assigned to target genes exactly as described20.

Ikaros Bio-ChIP-sequencing resulted in ~180 million reads. To make these data comparable with other, less deeply sequenced ChIP-seq data, we implemented a subsampling procedure as follows: Both the input and Ikaros ChIP-seq data were down-sampled randomly 10 times to 27.3 and 22.5 million reads, respectively. These read numbers were selected to match those of the previously published DHS-seq data20 and input sequences. Peaks were then called for all Ikaros ChIP-seq and input subsample combinations (10x10), as described above. The 9878 Ikaros peaks, which were called in 80% of all combinations, were used for multiple peak overlap analysis based on the Multovl program21.

Peak overlap analysis

All peak overlap analyses were performed with the Multovl program21 by using a minimal overlap length of one and allowing for all possible overlaps. Results were parsed and converted to tables with custom-made bash, perl and R scripts and analyzed using the TIPCO Spotfire program (version 5.0.1).

De novo motif discovery

We selected the top 300 Ikaros peaks from the Bio-ChIP-seq data of pro-B and DP T cells for de novo motif discovery. The ranking of the peaks was performed based on the ratio of the read counts between the peak and adjacent sequences and the identification of similar peak summits by the three different methods MACS, SISSRS and extend Coverage (as implemented in the Chipseq R package; version 2.15.3). The 300 nucleotides centered at the resulting peak summit were submitted to the MEME-ChIP motif discovery tool (version 4.9.0.2rc5)22. We allowed for a range of motif widths (4-12 nucleotides), number of sites (2-150) and repetitions (oops, zoops and anr options), and reported the best five motifs together with their significance as determined by the E-value. The resulting Ikaros motifs were very similar, irrespective of the parameters used.

Analysis of pro-B cell RNA-seq data

For analysis of differential gene expression, the RNA-seq samples were cut down to a read length of 30 or 44 bp (depending on the RNA-seq experiments to be compared) and aligned to the mouse transcriptome using the TopHat version 1.4.1 (ref. 23). The number of reads per gene was counted using the HTseq version 0.5.3 (http://www-huber.embl.de/users/anders/HTSeq) with the overlap resolution mode option set to ‘union’. As two independent RNA-seq experiments were available for each cell type analyzed in Fig. 3f-h and Fig. 8b, the corresponding RNA-seq data were compared by using the R package DESeq version 1.8.3 (ref. 24) to calculate the significance level of differential expression. To this end, the samples were normalized, and the dispersions were estimated using the default DESeq settings. Genes with an adjusted p-value of < 0.1 were called as differentially expressed.

Analysis of pre-pro-B cell RNA-seq data

The RNA-seq data of the 16 shRNA experiments (Supplementary Table 2) were analyzed together. Justified by the observed similarity, the samples of the pre-pro-B cells expressing the Ren713 shRNA or empty retroviral vector were treated as control replicas. All samples were RLE-normalized24,25 to adjust for the differences in the active library sizes. The dispersions were sequentially estimated by the edgeR package version 3.2.1 (ref. 25) using the default settings. First, a common dispersion for the gene set was estimated, and the tagwise dispersion values were then shrunken towards this dispersion trend26. The edgeR package version 3.2.1 (ref. 25) was used for the statistical modeling and analysis. Due to the experimental paired-sample design, a model taking both the different infection efficiencies and the individual shRNA effects into account was fitted. The significance of the gene-specific shRNA coefficient (referred to as adjusted counts in Fig. 8e) was statistically tested, and the p-values were corrected for multiple testing using the Benjamini-Hochberg adjustment27. Genes with an adjusted p-value of less then 0.1 were called as statistically significant. In addition, a fold change threshold of 3 was applied to define the repressed genes, whereas a threshold of 2 was used for the activated genes.

Supplementary Material

Refer to Web version on PubMed Central for supplementary material.

Acknowledgements

We thank G. Schmauß, T. Lendl and G. Stengl for FACS sorting, C. Theussl and J. Wojciechowski for blastocyst injection, B. Vilagos for providing the EBF1 ChIP-seq data, K. Georgopoulos for the *Ikzf1*$^{+/-}$ mouse, H. Karasuyama for the anti-Igβ antibody, and A. Sommer and his team at the Campus Science Support Facilities for Illumina sequencing. This research was supported by Boehringer Ingelheim, an ERC Advanced Grant (291740-LymphoControl) from the European Community's Seventh Framework Program and the Austrian GEN-AU initiative (financed by the Bundesminsterium für Bildung und Wissenschaft) and an EMBO fellowship (to TAS).

References

1. Georgopoulos K. Haematopoietic cell-fate decisions, chromatin regulation and Ikaros. Nature Rev Immunol. 2002; 2:162–174. [PubMed: 11913067]
2. Wang J-H, et al. Selective defects in the development of the fetal and adult lymphoid system in mice with an Ikaros null mutation. Immunity. 1996; 5:537–549. [PubMed: 8986714]
3. Mullighan CG, et al. *BCR-ABL1* lymphoblastic leukaemia is characterized by the deletion of Ikaros. Nature. 2008; 453:110–114. [PubMed: 18408710]
4. Mullighan CG, et al. Deletion of *IKZF1* and prognosis in acute lymphoblastic leukemia. N Engl J Med. 2009; 360:470–480. [PubMed: 19129520]
5. Ng SY-M, Yoshida T, Zhang J, Georgopoulos K. Genome-wide lineage-specific transcriptional networks underscore Ikaros-dependent lymphoid priming in hematopoietic stem cells. Immunity. 2009; 30:493–507. [PubMed: 19345118]
6. Yoshida T, Ng SY-M, Zúñiga-Pflücker JC, Georgopoulos K. Early hematopoietic lineage restrictions directed by Ikaros. Nat Immunol. 2006; 7:382–391. [PubMed: 16518393]
7. Kirstetter P, Thomas M, Dierich A, Kastner P, Chan S. Ikaros is critical for B cell differentiation and function. Eur J Immunol. 2002; 32:720–730. [PubMed: 11870616]
8. Schjerven H, et al. Selective regulation of lymphopoiesis and leukemogenesis by individual zinc fingers of Ikaros. Nat Immunol. 2013; 14:1073–1083. [PubMed: 24013668]
9. Herzog S, Reth M, Jumaa H. Regulation of B-cell proliferation and differentiation by pre-B-cell receptor signalling. Nat Rev Immunol. 2009; 9:195–205. [PubMed: 19240758]
10. Thompson EC, et al. Ikaros DNA-binding proteins as integral components of B cell developmental-stage-specific regulatory circuits. Immunity. 2007; 26:335–344. [PubMed: 17363301]
11. Ma S, Pathak S, Trinh L, Lu R. Interferon regulatory factors 4 and 8 induce the expression of Ikaros and Aiolos to down-regulate pre-B-cell receptor and promote cell-cycle withdrawal in pre-B-cell development. Blood. 2008; 111:1396–1403. [PubMed: 17971486]
12. Mandal M, et al. Ras orchestrates exit from the cell cycle and light-chain recombination during early B cell development. Nat Immunol. 2009; 10:1110–1117. [PubMed: 19734904]
13. Trageser D, et al. Pre-B cell receptor-mediated cell cycle arrest in Philadelphia chromosome-positive acute lymphoblastic leukemia requires *IKAROS* function. J Exp Med. 2009; 206:1739–1753. [PubMed: 19620627]
14. Ma S, et al. Ikaros and Aiolos inhibit pre-B-cell proliferation by directly suppressing c-Myc expression. Mol Cell Biol. 2010; 30:4149–4158. [PubMed: 20566697]
15. Ferreirós-Vidal I, et al. Genome-wide identification of Ikaros targets elucidates its contribution to mouse B-cell lineage specification and pre-B-cell differentiation. Blood. 2013; 121:1769–1782. [PubMed: 23303821]
16. Sun L, Liu A, Georgopoulos K. Zinc finger-mediated protein interactions modulate Ikaros activity, a molecular control of lymphocyte development. EMBO J. 1996; 15:5358–5369. [PubMed: 8895580]
17. Hobeika E, et al. Testing gene function early in the B cell lineage in mb1-cre mice. Proc Natl Acad Sci USA. 2006; 103:13789–13794. [PubMed: 16940357]
18. Kwon K, et al. Instructive role of the transcription factor E2A in early B lymphopoiesis and germinal center B cell development. Immunity. 2008; 28:751–762. [PubMed: 18538592]
19. Shinkai Y, et al. RAG-2-deficient mice lack mature lymphocytes owing to inability to initiate V(D)J rearrangement. Cell. 1992; 68:855–867. [PubMed: 1547487]

20. Revilla-i-Domingo R, et al. The B-cell identity factor Pax5 regulates distinct transcriptional programmes in early and late B lymphopoiesis. EMBO J. 2012; 31:3130–3146. [PubMed: 22669466]
21. Molnár A, Georgopoulos K. The Ikaros gene encodes a family of functionally diverse zinc finger DNA-binding proteins. Mol Cell Biol. 1994; 14:8292–8303. [PubMed: 7969165]
22. Zhang J, et al. Harnessing of the nucleosome-remodeling-deacetylase complex controls lymphocyte development and prevents leukemogenesis. Nat Immunol. 2012; 13:86–94.
23. Morgan B, et al. Aiolos, a lymphoid restricted transcription factor that interacts with Ikaros to regulate lymphocyte differentiation. EMBO J. 1997; 16:2004–2013. [PubMed: 9155026]
24. Nagata K, et al. The Igα/Igβ heterodimer on μ-negative proB cells is competent for transducing signals to induce early B cell differentiation. Immunity. 1997; 7:559–570. [PubMed: 9354476]
25. Carninci P, et al. Genome-wide analysis of mammalian promoter architecture and evolution. Nat Genet. 2006; 38:626–635. [PubMed: 16645617]
26. Vilagos B, et al. Essential role of EBF1 in the generation and function of distinct mature B cell types. J Exp Med. 2012; 209:775–792. [PubMed: 22473956]
27. Kim J, et al. Ikaros DNA-binding proteins direct formation of chromatin remodeling complexes in lymphocytes. Immunity. 1999; 10:345–355. [PubMed: 10204490]
28. Sridharan R, Smale ST. Predominant interaction of both Ikaros and Helios with the NuRD complex in immature thymocytes. J Biol Chem. 2007; 282:30227–30238. [PubMed: 17681952]
29. Zuber J, et al. Toolkit for evaluating genes required for proliferation and survival using tetracycline-regulated RNAi. Nat Biotechnol. 2011; 29:79–83. [PubMed: 21131983]
30. Fellmann C, et al. An optimized microRNA backbone for effective single-copy RNAi. Cell Rep. 2014; 5:1704–1713.
31. Wang JH, et al. *Aiolos* regulates B cell activation and maturation to effector state. Immunity. 1998; 9:543–553. [PubMed: 9806640]
32. Karnowski A, et al. Silencing and nuclear repositioning of the λ5 gene locus at the pre-B cell stage requires Aiolos and OBF-1. PLoS One. 2008; 3:e3568. [PubMed: 18974788]
33. Gómez-del Arco P, Koipally J, Georgopoulos K. Ikaros SUMOylation: switching out of repression. Mol Cell Biol. 2005; 25:2688–2697. [PubMed: 15767674]
34. Fuxa M, Busslinger M. Reporter gene insertions reveal a strictly B lymphoid-specific expression pattern of *Pax5* in support of its B cell identity function. J Immunol. 2007; 178:8222–8228. [PubMed: 17600970]
35. van Rijssel J, et al. The Rho-guanine nucleotide exchange factor Trio controls leukocyte transendothelial migration by promoting docking structure formation. Mol Biol Cell. 2012; 23:2831–2844. [PubMed: 22696684]
36. Brugnera E, et al. Unconventional Rac-GEF activity is mediated through the Dock180-ELMO complex. Nat Cell Biol. 2002; 4:574–582. [PubMed: 12134158]
37. Pearce G, et al. Signaling protein SWAP-70 is required for efficient B cell homing to lymphoid organs. Nat Immunol. 2006; 7:827–834. [PubMed: 16845395]
38. Rooney C, et al. The Rac activator STEF (Tiam2) regulates cell migration by microtubule-mediated focal adhesion disassembly. EMBO Rep. 2010; 11:292–298. [PubMed: 20224579]
39. Pasteris NG, et al. Isolation and characterization of the faciogenital dysplasia (Aarskog-Scott syndrome) gene: a putative Rho/Rac guanine nucleotide exchange factor. Cell. 1994; 79:669–678. [PubMed: 7954831]
40. Cai D, et al. AND-34/BCAR3, a GDP exchange factor whose overexpression confers antiestrogen resistance, activates Rac, PAK1, and the cyclin D1 promoter. Cancer Res. 2003; 63:6802–6808. [PubMed: 14583477]
41. Miyamoto Y, Yamauchi J, Sanbe A, Tanoue A. Dock6, a Dock-C subfamily guanine nucleotide exchanger, has the dual specificity for Rac1 and Cdc42 and regulates neurite outgrowth. Exp Cell Res. 2007; 313:791–804. [PubMed: 17196961]
42. Tokoyoda K, Egawa T, Sugiyama T, Choi B-I, Nagasawa T. Cellular niches controlling B lymphocyte behavior within bone marrow during development. Immunity. 2004; 20:707–718. [PubMed: 15189736]

43. Koipally J, Georgopoulos K. Ikaros interactions with CtBP reveal a repression mechanism that is independent of histone deacetylase activity. J Biol Chem. 2000; 275:19594–19602. [PubMed: 10766745]
44. Koipally J, Renold A, Kim J, Georgopoulos K. Repression by Ikaros and Aiolos is mediated through histone deacetylase complexes. EMBO J. 1999; 18:3090–3100. [PubMed: 10357820]
45. Koipally J, Georgopoulos K. A molecular dissection of the repression circuitry of Ikaros. J Biol Chem. 2002; 277:27697–27705. [PubMed: 12015313]
46. Dupuis A, et al. Biclonal and biallelic deletions occur in 20% of B-ALL cases with IKZF1 mutations. Leukemia. 2013; 27:503–507. [PubMed: 22868967]
47. Heltemes-Harris LM, et al. *Ebf1* or *Pax5* haploinsufficiency synergizes with STAT5 activation to initiate acute lymphoblastic leukemia. J Exp Med. 2011; 208:1135–1149. [PubMed: 21606506]

Online Methods References

1. Wang J-H, et al. Selective defects in the development of the fetal and adult lymphoid system in mice with an Ikaros null mutation. Immunity. 1996; 5:537–549. [PubMed: 8986714]
2. Lin H, Grosschedl R. Failure of B-cell differentiation in mice lacking the transcription factor EBF. Nature. 1995; 376:263–267. [PubMed: 7542362]
3. Vilagos B, et al. Essential role of EBF1 in the generation and function of distinct mature B cell types. J Exp Med. 2012; 209:775–792. [PubMed: 22473956]
4. Driegen S, et al. A generic tool for biotinylation of tagged proteins in transgenic mice. Transgenic Res. 2005; 14:477–482. [PubMed: 16201414]
5. Shinkai Y, et al. RAG-2-deficient mice lack mature lymphocytes owing to inability to initiate V(D)J rearrangement. Cell. 1992; 68:855–867. [PubMed: 1547487]
6. Hobeika E, et al. Testing gene function early in the B cell lineage in mb1-cre mice. Proc Natl Acad Sci USA. 2006; 103:13789–13794. [PubMed: 16940357]
7. Tallquist MD, Soriano P. Epiblast-restricted Cre expression in MORE mice: a tool to distinguish embryonic vs. extra-embryonic gene function. Genesis. 2000; 26:113–115. [PubMed: 10686601]
8. Schlenner SM, et al. Fate mapping reveals separate origins of T cells and myeloid lineages in the thymus. Immunity. 2010; 32:426–436. [PubMed: 20303297]
9. de Boer J, et al. Transgenic mice with hematopoietic and lymphoid specific expression of Cre. Eur J Immunol. 2003; 33:314–325. [PubMed: 12548562]
10. Rodriguez CI, et al. High-efficiency deleter mice show that FLPe is an alternative to Cre-*loxP*. Nat Genet. 2000; 25:139–140. [PubMed: 10835623]
11. de Boer E, et al. Efficient biotinylation and single-step purification of tagged transcription factors in mammalian cells and transgenic mice. Proc Natl Acad Sci USA. 2003; 100:7480–7485. [PubMed: 12802011]
12. Nutt SL, Urbánek P, Rolink A, Busslinger M. Essential functions of Pax5 (BSAP) in pro-B cell development: difference between fetal and adult B lymphopoiesis and reduced *V*-to-*DJ* recombination at the *IgH* locus. Genes Dev. 1997; 11:476–491. [PubMed: 9042861]
13. Decker T, et al. Stepwise activation of enhancer and promoter regions of the B cell commitment gene *Pax5* in early lymphopoiesis. Immunity. 2009; 30:508–520. [PubMed: 19345119]
14. Zuber J, et al. Toolkit for evaluating genes required for proliferation and survival using tetracycline-regulated RNAi. Nat Biotechnol. 2011; 29
15. Fellmann C, et al. An optimized microRNA backbone for effective single-copy RNAi. Cell Rep. 2014; 5:1704–1713.
16. Schebesta A, et al. Transcription factor Pax5 activates the chromatin of key genes involved in B cell signaling, adhesion, migration and immune function. Immunity. 2007; 27:49–63. [PubMed: 17658281]
17. Ebert A, et al. The distal V_H gene cluster of the *Igh* locus contains distinct regulatory elements with Pax5 transcription factor-dependent activity in pro-B cells. Immunity. 2011; 34:175–187. [PubMed: 21349430]

18. Parkhomchuk D, et al. Transcriptome analysis by strand-specific sequencing of complementary DNA. Nucleic Acids Res. 2009; 37:e123. [PubMed: 19620212]
19. Zhang Y, et al. Model-based analysis of ChIP-Seq (MACS). Genome Biol. 2008; 9:R137. [PubMed: 18798982]
20. Revilla-i-Domingo R, et al. The B-cell identity factor Pax5 regulates distinct transcriptional programmes in early and late B lymphopoiesis. EMBO J. 2012; 31:3130–3146. [PubMed: 22669466]
21. Aszódi A. MULTOVL: fast multiple overlaps of genomic regions. Bioinformatics. 2012; 28:3318–3319. [PubMed: 23071271]
22. Bailey TL, et al. MEME SUITE: tools for motif discovery and searching. Nucleic Acids Res. 2009; 37
23. Trapnell C, Pachter L, Salzberg SL. TopHat: discovering splice junctions with RNA-Seq. Bioinformatics. 2009; 25:1105–1111. [PubMed: 19289445]
24. Anders S, Huber W. Differential expression analysis for sequence count data. Genome Biol. 2010; 11:R106. [PubMed: 20979621]
25. Robinson MD, McCarthy DJ, Smyth GK. edgeR: a Bioconductor package for differential expression analysis of digital gene expression data. Bioinformatics. 2010; 26:139–140. [PubMed: 19910308]
26. McCarthy DJ, Chen Y, Smyth GK. Differential expression analysis of multifactor RNA-Seq experiments with respect to biological variation. Nucleic Acids Res. 2012; 40:4288–4297. [PubMed: 22287627]
27. Benjamini Y, Hochberg Y. Controlling the false discovery rate: a practical and powerful approach to multiple testing. J Royal Statistical Society. 1995; 57:289–300.

Europe PMC Funders Author Manuscripts

Europe PMC Funders Author Manuscripts

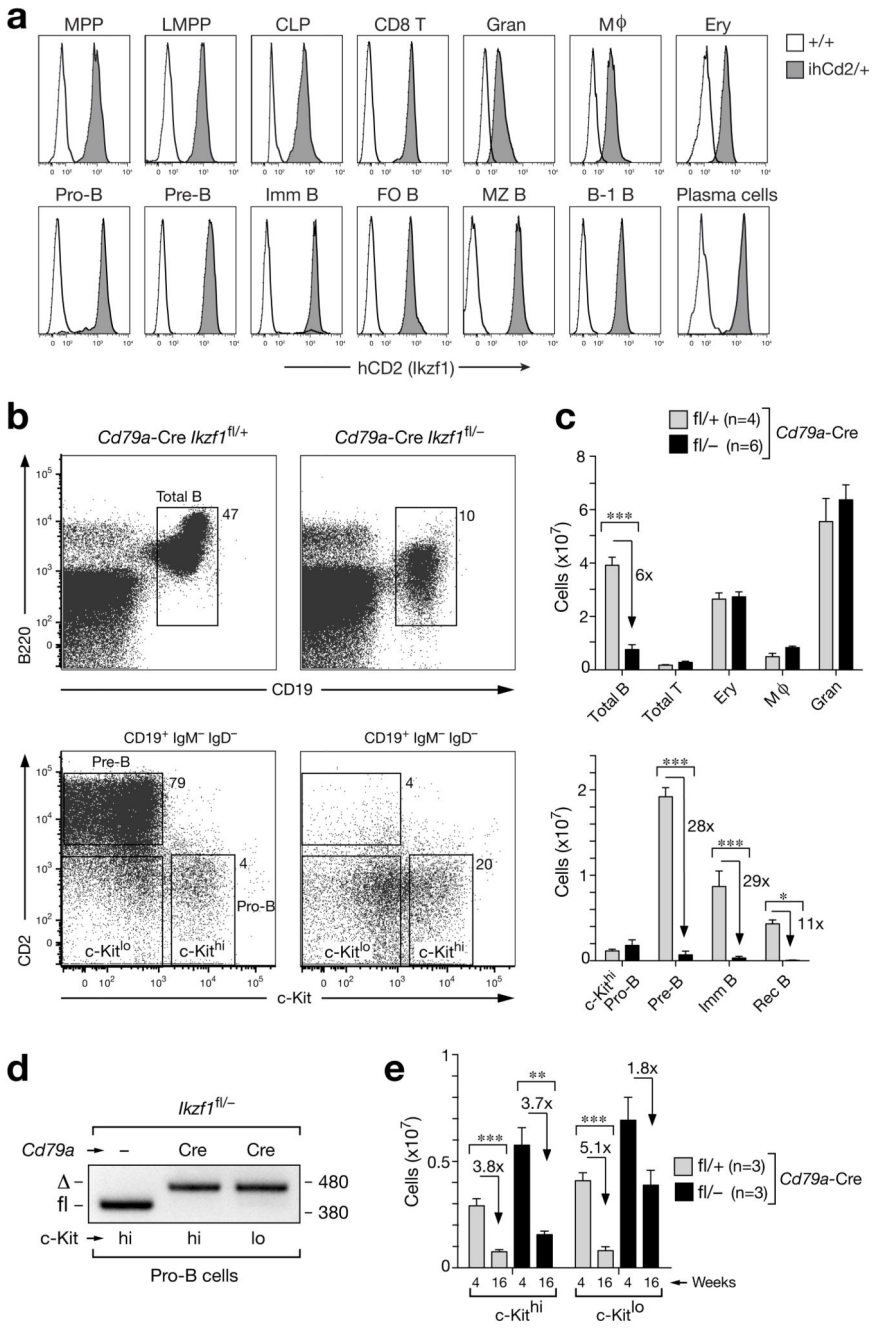

Figure 1. Ikaros loss in pro-B cells arrests development at the pro-B to pre-B cell transition.

(**a**) Flow cytometry analysis of human (h) CD2 expression in different hematopoietic cell types (defined in Online Methods) of *Ikzf1*$^{ihCd2/+}$ (grey) and wild-type (black line) mice. Follicular (FO) B, marginal zone (MZ) B, B-1 B and CD8 T cells were isolated from the spleen, whereas bone marrow was used to analyze all other cell types. MPP, multipotent progenitor; LMPP, lymphoid-primed multipotent progenitors; CLP, common lymphoid progenitor; Imm, immature; Gran, granulocyte; M**ϕ**, macrophage; Ery, erythroblast. (**b**,**c**) Flow cytometry (**b**) and absolute numbers (**c**) of the indicated cell types in bone marrow

isolated from the femur and tibia of the two hind legs of 6-8-week-old *Cd79a*-Cre *Ikzf1*$^{fl/+}$ mice (grey bars) and *Cd79a*-Cre *Ikzf1*$^{fl/-}$ littermates (black bars). Numbers refer to percent cells in the indicated gate (**b**), and *n* indicates the number of mice analyzed (**c**). Statistical data (**c**) are shown with SEM and were analyzed by two-way analysis of variance (ANOVA) with Bonferoni's post-test; * ($p < 0.05$), ** ($p < 0.01$), *** ($p < 0.001$). (**d**) Deletion of the floxed *Ikzf1* allele in ex vivo sorted c-Kit^{hi} and c-Kit^{lo} pro-B cells from *Cd79a*-Cre *Ikzf1*$^{fl/-}$ and control *Ikzf1*$^{fl/-}$ mice. PCR fragments corresponding to the deleted (Δ) or intact (fl) floxed allele are indicated to the left and their size (in base pairs) to the right of the PCR gel. (**e**) Age-dependent pro-B cell numbers. Absolute numbers are shown for c-Kit^{hi} and c-Kit^{lo} pro-B cells (CD19^{+}CD25^{-}IgM^{-}IgD^{-}) in the bone marrow of *Cd79a*-Cre *Ikzf1*$^{fl/+}$ (grey bar) and *Cd79a*-Cre *Ikzf1*$^{fl/-}$ (black bar) mice at the age of 4 and 16 weeks. Statistical data (**e**) are shown with SEM and were analyzed by the Student *t*-test (two-tailed, unpaired); * ($p < 0.05$), ** ($p < 0.01$), *** ($p < 0.001$).

Europe PMC Funders Author Manuscripts

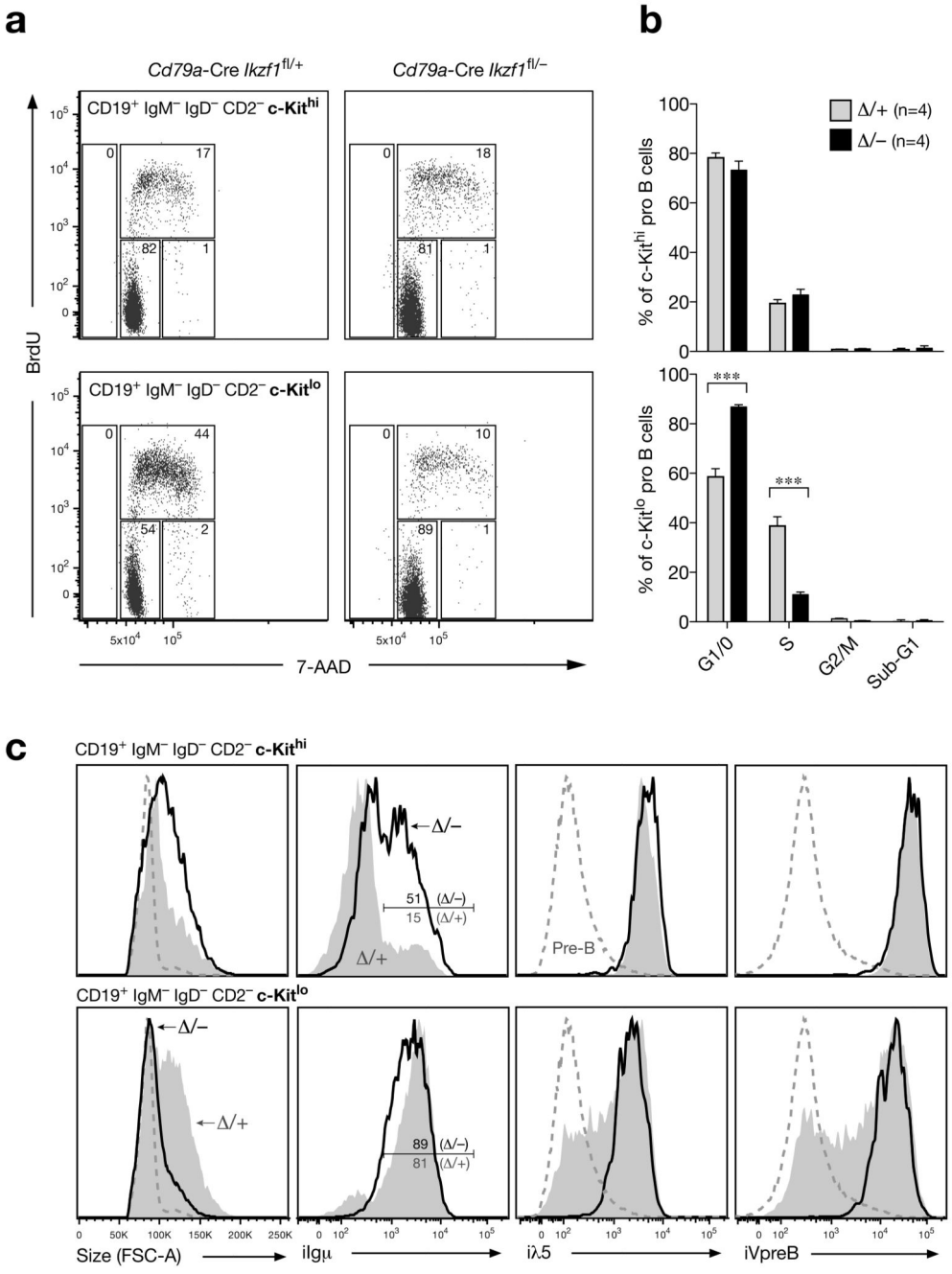

Figure 2. Cell cycle arrest of Ikaros-deficient c-Kit^{lo} 'pro-B' cells despite Igμ expression.

(**a, b**) Cell cycle analysis. Following intraperitoneal injection of BrdU for 40 minutes, the bone marrow of 5-8-week-old mice was stained for cell surface proteins and subsequently fixed, permeabilized and DNase I-treated prior to detection of total DNA with 7-AAD and incorporated BrdU with BrdU antibodies. c-Kit^{hi} (upper panel) and c-Kit^{lo} (lower panel) CD19^{+}CD2$^{–}$IgM$^{–}$IgD$^{–}$ cells from experimental *Cd79a*-Cre *Ikzf1*$^{fl/–}$ mice (Δ/–; black bars) and control *Cd79a*-Cre *Ikzf1*$^{fl/+}$ mice (Δ/+; grey bars) were analyzed by flow cytometry for DNA content and BrdU incorporation. Representative FACS plots (**a**) are shown together

with the average percentage of cells in the different cell cycle phases (**b**). *n* indicates the number of mice analyzed. Statistical data (**b**) are shown with SEM and were analyzed by two-way analysis of variance (ANOVA) with Bonferoni's post-test; *** ($p < 0.001$). (**c**) Flow cytometric analysis. c-Kit^{hi} and c-Kit^{lo} CD19^{+}CD2^{-}IgM^{-}IgD^{-} cells from the bone marrow of experimental *Cd79a*-Cre *Ikzf1*$^{fl/-}$ mice (black line) and control *Cd79a*-Cre *Ikzf1*$^{fl/+}$ littermates (grey) were analyzed for cell size (FSC-A) and expression of Igμ, λ5 and VpreB by intracellular staining. Small pre-B cells (c-Kit$^{lo/-}$CD19^{+}CD2^{+}IgM^{-}IgD^{-}; dashed line) of control *Cd79a*-Cre *Ikzf1*$^{fl/+}$ mice are shown for comparison.

Europe PMC Funders Author Manuscripts

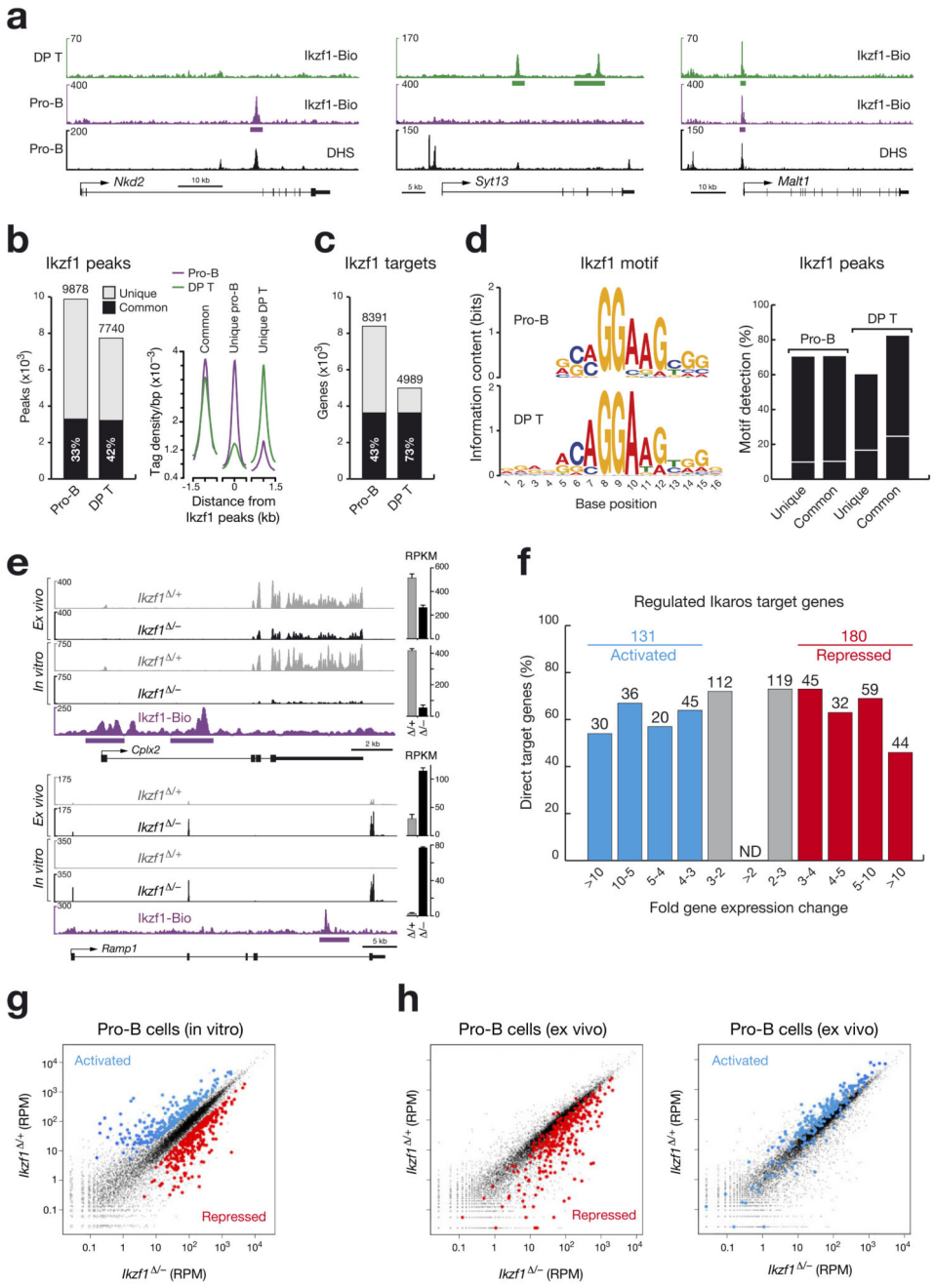

Figure 3. Identification of regulated Ikaros target genes in pro-B cells.

(**a**) Ikaros binding at unique and common sites in pro-B cells and CD4^{+}CD8^{+} double-positive (DP) thymocytes. Ikaros-binding sites were identified by Bio-ChIP-sequencing of *Ikzf1*$^{ihCd2/ihCd2}$ *Rosa26*$^{BirA/BirA}$ *Rag2*$^{-/-}$ pro-B cells (purple) and *Ikzf1*$^{ihCd2/ihCd2}$ *Rosa26*$^{BirA/BirA}$ DP T cells (green). Genes with unique and common Ikaros-binding sites are shown together with their DNase I hypersensitive (DHS) sites20, exon-intron structure and a scale bar shown in kilobases (kb). Bars below the ChIP-seq track indicate Ikaros-binding regions identified by MACS peak calling. (**b**) Number and overlap of Ikaros peaks in pro-B

and DP T cells. Total numbers of 9,878 and 7,740 Ikaros peaks with an overlap of 3,293 common peaks (black bar) were identified in pro-B and DP T cells, respectively, by using a p-value of $< 10^{-10}$ for peak calling. Average sequence tag density profiles aligned at the center of the Ikaros peaks are shown for common and unique Ikaros-binding sites in the two cell types (right). (**c**) Identification of common and unique Ikaros target genes in pro-B and DP T cells by peak-to-gene assignment as described20. (**d**) Consensus Ikaros recognition sequence identified by de novo motif discovery in pro-B and DP T cells. The respective motifs had E-values of $1.8x10^{-59}$ (pro-B) and $7.8x10^{-142}$ (DP T) and were detected at the indicated frequency (%) in common and unique Ikaros peaks of pro-B and DP T cells, respectively (right). The same motifs were found in random DNA sequences at the frequency indicated by a white line. (**e**) Expression of the two regulated Ikaros target genes *Cplx2* and *Ramp1* in short-term in vitro cultured and ex vivo sorted pro-B cells of *Cd79a*-Cre *Ikzf1*$^{fl/-}$ (*Ikzf1*$^{\Delta/-}$; black) and *Cd79a*-Cre *Ikzf1*$^{fl/+}$ (*Ikzf1*$^{\Delta/+}$; grey) mice, as determined by RNA-seq. Normalized expression values are indicated as RPKMs (plus SEM) to the right. Ikaros peaks were identified by Bio-ChIP-seq. (**f**) Identification of activated and repressed Ikaros target genes in short-term cultured pro-B cells. The number and percentage of Ikaros target genes are shown for the indicated fold gene expression differences between experimental *Ikzf1*$^{\Delta/-}$ and control *Ikzf1*$^{\Delta/+}$ pro-B cells. For evaluation of the RNA-seq data, see Online Methods. Activated and repressed genes were further selected for an RPKM value of > 5 in control *Ikzf1*$^{\Delta/+}$ pro-B cells (activated) or *Ikzf1*$^{\Delta/-}$ pro-B cells (repressed), respectively (Supplementary Table 1). ND, not determined. (**g**) Scatter plot of gene expression differences observed between in vitro cultured *Ikzf1*$^{\Delta/-}$ and *Ikzf1*$^{\Delta/+}$ pro-B cells. The normalized expression data of individual genes in the two pro-B cell types were plotted as RPM (*r*eads *p*er gene per *m*illion mapped sequence tags) values. Each dot represents one gene. Activated and repressed Ikaros target genes, which were identified as described in (**f**), are colored in blue or red, respectively. (**h**) Scatter plot of gene expression changes determined in ex vivo sorted *Ikzf1*$^{\Delta/-}$ and *Ikzf1*$^{\Delta/+}$ pro-B cells. Genes in the ex vivo RNA-seq data, which correspond to the activated and repressed Ikaros target genes identified in in vitro cultured pro-B cells (**f**), are colored in blue and red, respectively.

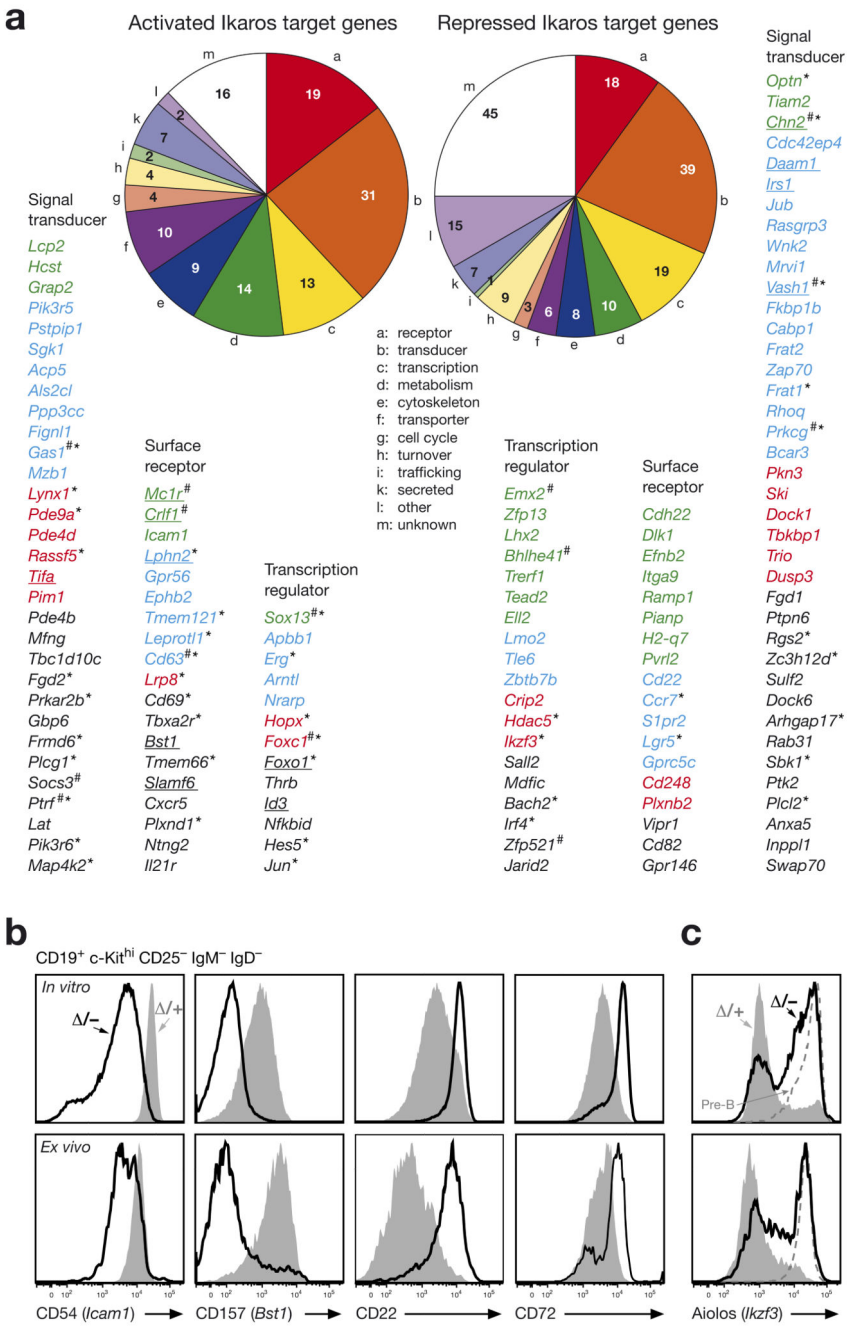

Figure 4. Function of activated and repressed Ikaros target genes in pro-B cells.

(**a**) Pie diagram indicating the different functional classes of activated and repressed Ikaros target genes in pro-B cells. Regulated Ikaros target genes coding for cell surface protein, signal transducer and transcription factors are shown below and ranked according to their fold expression changes observed between in vitro cultured *Ikzf1*$^{\Delta/-}$ and *Ikzf1*$^{\Delta/+}$ pro-B cells (Fig. 3f; Supplementary Table 1). The color code refers to >10-fold (green), 5-10-fold (blue), 4-5-fold (red) and 3-4-fold (black). Underlined target genes were jointly activated or repressed by Ikaros and Pax5 (ref. 20). The number sign (#) indicates genes with low

Europe PMC Funders Author Manuscripts

expression levels in ex vivo sorted pro-B cells, i.e. < 5 RPKM in *Ikzf1*$^{\Delta/+}$ pro-B cells for activated target genes and < 5 RPKM in *Ikzf1*$^{\Delta/-}$ pro-B cells for repressed target gene. Asterisks indicate genes, which were not regulated (< 1.4-fold) in short-term cultured *Ikzf1*$^{\Delta/-}$ *Rag2*$^{-/-}$ and *Ikzf1*$^{\Delta/+}$ *Rag2*$^{-/-}$ pro-B cells. (**b**) Validation of regulated Ikaros target genes at the protein level. In vitro cultured and ex vivo c-Kit^{hi} pro-B cells (CD19^{+}CD2^{-} IgM^{-}IgD^{-}) of the *Cd79a*-Cre *Ikzf1*$^{fl/-}$ (Δ/–; black line) and *Cd79a*-Cre *Ikzf1*$^{fl/+}$ (Δ/+; grey) genotypes were analyzed by flow cytometry for the expression of cell surface proteins encoded by activated (*Icam1*, *Bst1*) and repressed (*Cd22*) target genes as well as by the indirectly repressed gene *Cd72*. (**c**) Aiolos expression in *Ikzf1* mutant pro-B cells. Aiolos expression was analyzed by intracellular staining of in vitro cultured and ex vivo c-Kit^{hi} pro-B cells (CD19^{+}CD2^{-}IgM^{-}IgD^{-}) from the *Cd79a*-Cre *Ikzf1*$^{fl/-}$ (Δ/–; black line) and *Cd79a*-Cre *Ikzf1*$^{fl/+}$ (Δ/+; grey) mice. Small pre-B cells (c-Kit^{-}CD19^{+}B220^{+}CD2^{+}IgM^{-}IgD^{-}; dashed line) of control mice are shown for comparison.

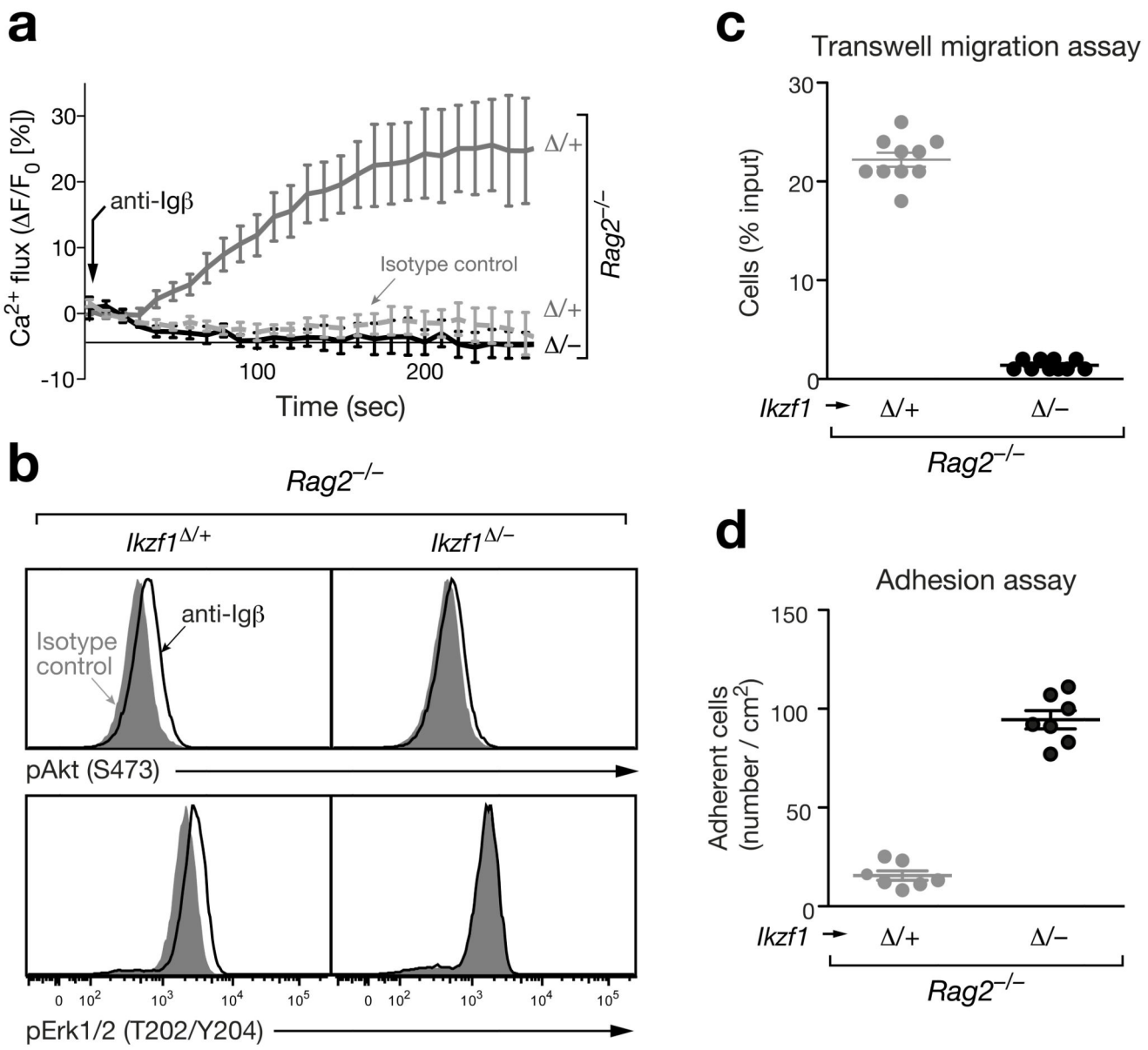

Figure 5. Ikaros controls pre-BCR signaling, cell migration and adhesion.

(**a**) Calcium signaling. Intracellular Ca^{2+} fluxes in *Cd79a*-Cre *Ikzf1*$^{fl/–}$ *Rag2*$^{–/–}$ or *Cd79a*-Cre *Ikzf1*$^{fl/+}$ *Rag2*$^{–/–}$ pro-B cells were recorded as an increase of the fluorescent emission of the Ca^{2+} sensor dye eFluor 524 (eBioscience) at 530/30 nm (excitation at 488 nm) after addition of the anti-Igβ antibody HM79 (arrow). An anti-TCRγδ antibody of the same isotype (hamster IgG2) was used as a control. (**b**) Signaling via the PI3K and MAPK pathways. Pro-B cell of the indicated genotypes were stimulated for 5 min with anti-Igβ or control anti-TCRγδ antibodies prior to flow cytometric assessment of the phosphorylation of Akt at Ser473 (pAkt) and Erk1/2 at Thr202/Tyr204 (pErk1/2). (**c**) Transwell migration assay. Pro-B cells of the indicated genotypes in IL-7-containing IMDM medium were placed in the upper compartment, whereas IL-7 medium containing 400 ng/ml CXCL12 (SDF-1α;

Sigma) was present in the lower compartment of a transwell chamber separated by a filter of 5 μm-pore size. Pro-B cells migrating into the lower chamber were measured after 2 hours in a Casy cell counter and are indicated as percentage of the total cells per well (shown as circle). The average percentage and SEM of three independent experiments are shown. (**d**) Adhesion assay. Pro-B cells of the indicated genotypes were allowed to adhere to VCAM1-Fc-coated glass slides in the presence of CXCL12 for 6 hours in IL-7-containing IMDM medium, washed 2 times and fixed in 4% paraformaldehyde (see Online Methods). Individual wells (shown as circles) of one experiment were evaluated by manual cell counting, and the average cell density with SEM is shown for pro-B cells of the indicated genotypes.

Europe PMC Funders Author Manuscripts

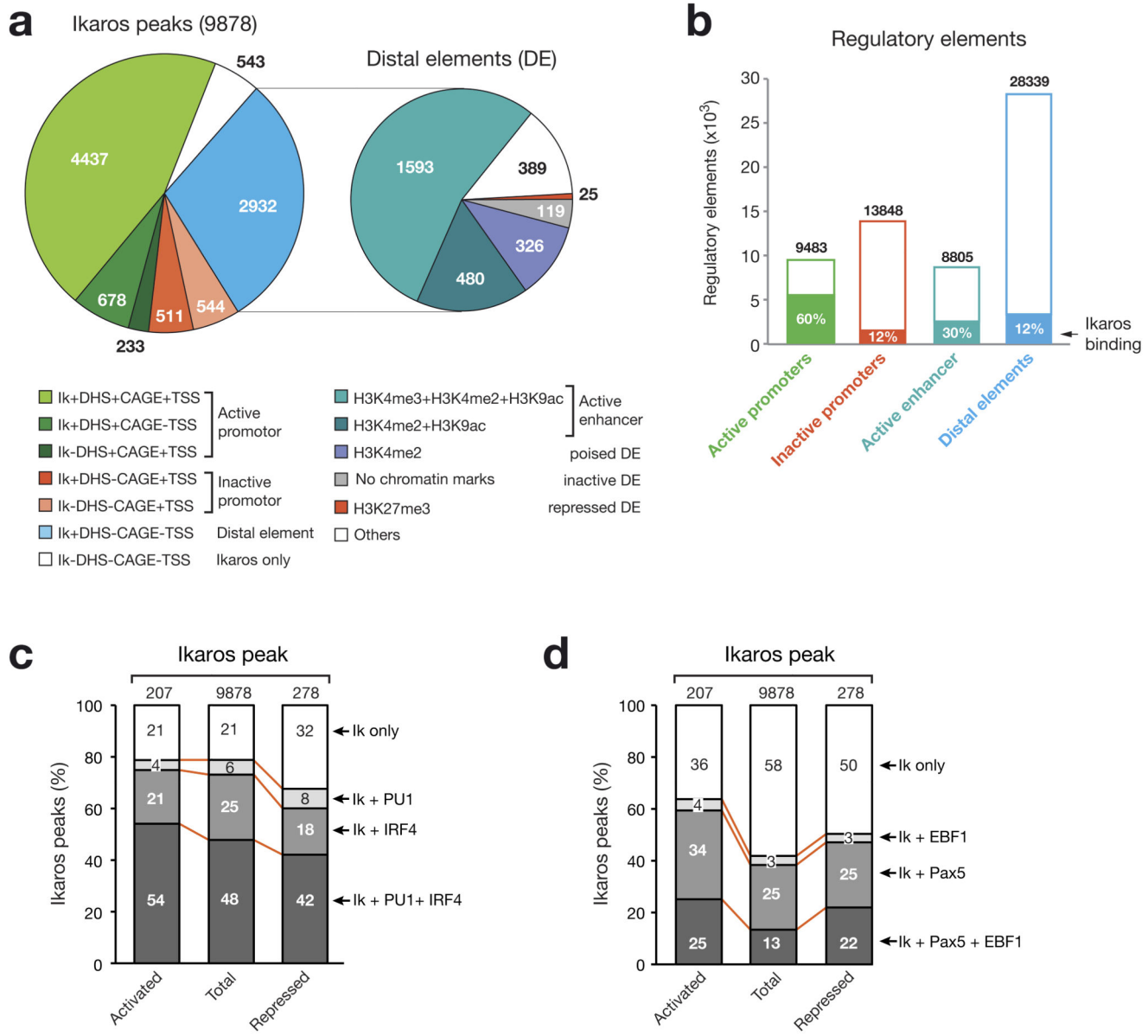

Figure 6. Overlap of Ikaros binding with the regulatory landscape and other transcription factor-binding sites in pro-B cells.

(**a**) Distribution of Ikaros (Ik) peaks at active and inactive promoters as well as distal elements. The regulatory landscape of *Rag2*$^{-/-}$ pro-B cells20 was previously determined by genome-wide mapping of DHS sites as well as active transcription start sites by the *c*ap *a*nalysis of *g*ene *e*xpression (CAGE) method25. TSS refers to mm9-annotated transcription start sites and CAGE to transcriptionally active TSSs. Non-annotated active promoters were defined by the category +DHS+CAGE-TSS. Distal elements (DE) were further subdivided into active enhancers as well as poised, inactive and repressed distal elements by genome-wide mapping of active (H3K4me2, H3K4me3, H3K9ac) and repressive (H3K27me3) histone marks20. (**b**) Relative enrichment of Ikaros-binding sites at distinct regulatory elements in *Rag2*$^{-/-}$ pro-B cells. The total number of the different elements is shown

Europe PMC Funders Author Manuscripts

together with the relative percentage of Ikaros binding. (**c,d**) Co-localization of Ikaros peaks with binding sites of PU.1 and IRF4 (**c**) or Pax5 and EBF1 (**d**). The co-occurrence of binding sites was determined by multiple overlap analysis of ChIP-seq data identifying binding of Pax5 (ref. 20), EBF1 (ref. 26), PU.1 (see Online Methods) and IRF4 (see Online Methods) in *Rag2*$^{-/-}$ pro-B cells. The overlap of binding sites is shown as percentage relative to total Ikaros-binding sites (Fig. 3b) and Ikaros-binding sites present at activated and repressed Ikaros target genes (Fig. 3f,g). Supplementary Fig. 6a shows examples of genes with overlapping transcription factor-binding sites.

Europe PMC Funders Author Manuscripts

Europe PMC Funders Author Manuscripts

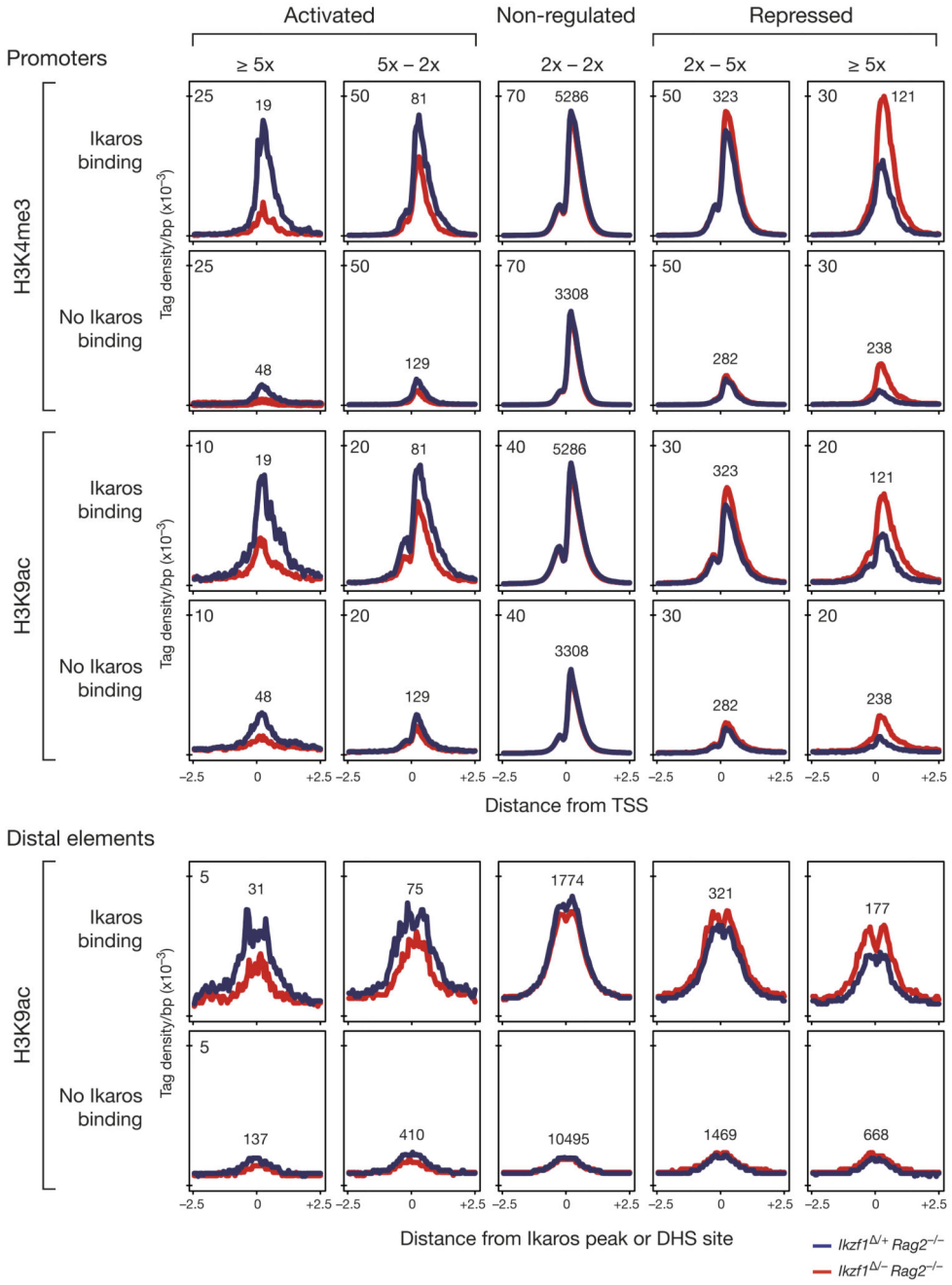

Figure 7. Chromatin changes at promoters and distal elements of Ikaros-regulated genes.

Ikaros-dependent chromatin changes were identified by ChIP-seq mapping of the active histone modifications H3K4me3 and H3K9ac in short-term cultured *Cd79a*-Cre *Ikzf1*$^{fl/-}$ *Rag2*$^{-/-}$ (red) and *Cd79a*-Cre *Ikzf1*$^{fl/+}$ *Rag2*$^{-/-}$ (blue) pro-B cells. Genes were classified according to their degree of Ikaros-dependent regulation (in the two *Rag2*$^{-/-}$ pro-B cell types) and the presence or absence of Ikaros-binding sites at their regulatory elements. The average density of the histone marks is shown for a region extending from -2.5 kb to +2.5 kb relative to the TSS at promoters or center of the Ikaros peak or DHS site (no Ikaros binding)

at distal elements. Only promoters and distal elements of genes with an expression level of > 2 RPKM in control pro-B cells (activated, not regulated) or in Ikaros-deficient pro-B cells (repressed) were analyzed. The number of peaks analyzed is shown for each category. Wilcoxon pair-matched comparison of the peak density at the regulatory elements in *Ikzf1*$^{\Delta/-}$ *Rag2*$^{-/-}$ and *Ikzf1*$^{\Delta/+}$ *Rag2*$^{-/-}$ pro-B cells revealed p-values of < 10^{-3} for all chromatin changes observed at promoters and distal elements of activated (> 2x) and repressed (> 2x) genes.

Europe PMC Funders Author Manuscripts

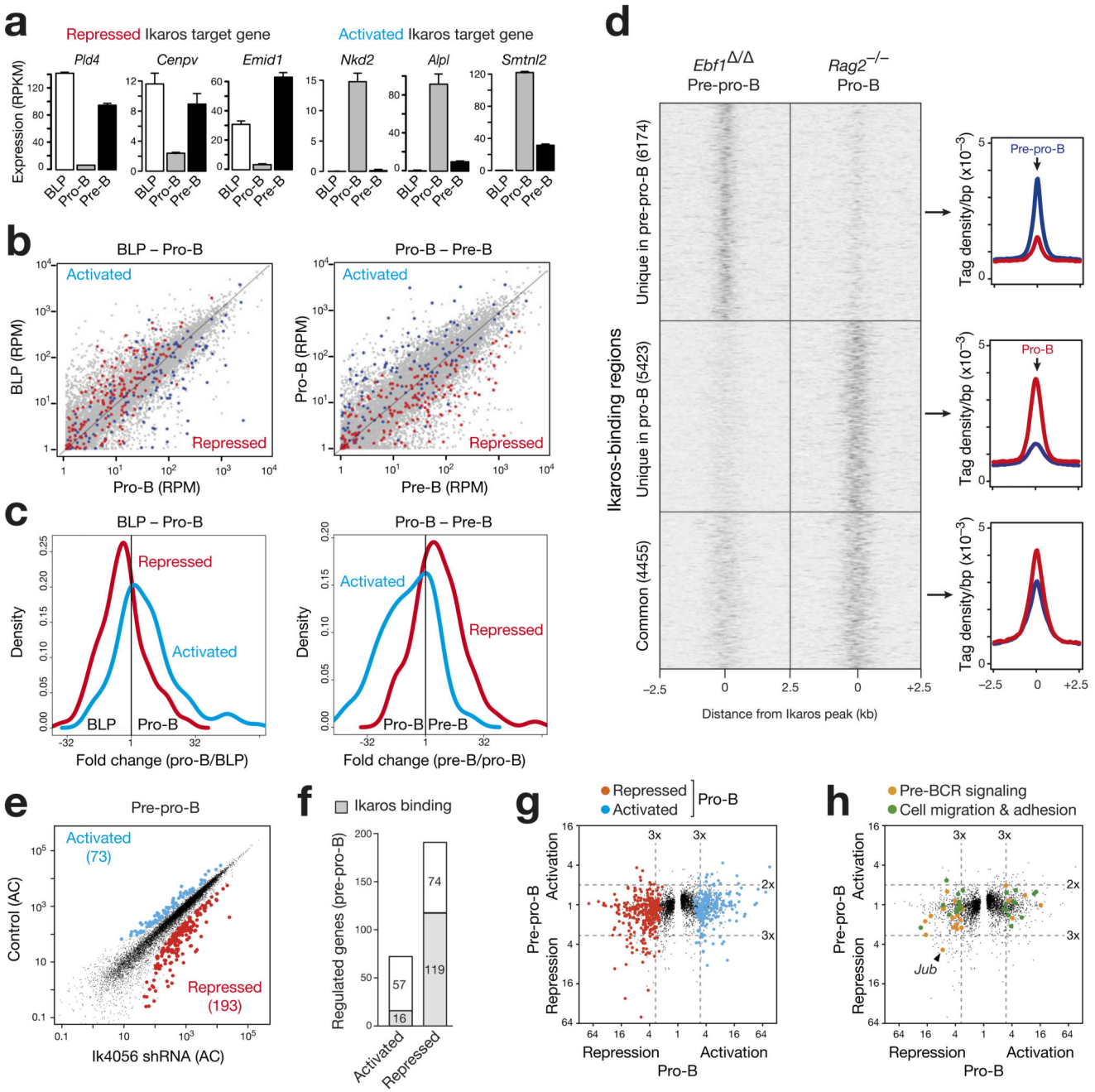

Figure 8. Ikaros regulates distinct target genes during early B-lymphopoiesis.

(**a**) Expression of selected repressed and activated Ikaros target genes during early B cell development. The expression of each gene in ex vivo sorted wild-type BLPs20, *Rag2*$^{-/-}$ pro-B cells20 and wild-type pre-B cells (this study) is shown as normalized expression value (RPKM) with SEM based on two independent RNA-seq experiments of each cell type. (**b**) Scatter plot of gene expression differences observed for the developmental transition from BLPs to pro-B cells and from pro-B to pre-B cells. Normalized expression data of individual genes in the two cell types were plotted as RPM values (grey dots), and the genes in these

RNA-seq data, which correspond to the 131 activated and 180 repressed Ikaros target genes identified in cultured pro-B cells (Fig. 3f,g), were colored as blue and red dots, respectively. (**c**) The fold expression change in the two developmental transitions is displayed as a density plot for the activated and repressed Ikaros target genes identified in pro-B cells. (**d**) Differential binding of Ikaros in pre-pro-B and pro-B cells. Ikaros binding in cultured *Vav*-Cre $Ebf1^{fl/fl}$ ($Ebf1^{\Delta/\Delta}$) $Ikzf1^{ihCd2/ihCd2}$ $Rosa26^{BirA/+}$ pre-pro-B cells was determined by Bio-ChIP-seq and compared to the Ikaros binding pattern of $Rag2^{-/-}$ pro-B cells (Fig. 3a,b). Unique and common Ikaros peaks of the two cell types are shown as heat maps (left) and density plots (right). (**e**) Scatter plot of gene expression differences between Ik4056 shRNA-expressing $Ebf1^{-/-}$ pre-pro-B cells and control $Ebf1^{-/-}$ pre-pro-B cells, which expressed either the Renilla luciferase Ren713 shRNA or empty retroviral vector. The expression of each gene in the experimental and control pre-pro-B cells was plotted as the corresponding adjusted count (AC; see Online Methods). Ikaros-activated genes (> 2-fold) and Ikaros-repressed genes (> 3-fold) with an adjusted p-value of < 0.1 are highlighted in blue and red, respectively. See Online Methods for detailed description of the shRNA experiments and bioinformatical analysis of the RNA-seq data. (**f**) Identification of activated and repressed Ikaros target genes in pre-pro-B cells. (**g**,**h**) Minimal overlap between regulated Ikaros target genes in pre-pro-B and pro-B cells. The fold expression change between $Ikzf1^{\Delta/-}$ and $Ikzf1^{\Delta/+}$ pro-B cells (x-axis) as well as between Ik4056 shRNA-expressing and control $Ebf1^{-/-}$ pre-pro-B cells (y-axis) is plotted for each gene. (**g**) The 131 activated and 180 repressed Ikaros target genes identified in pro-B cells (Fig. 3f,g) are colored as blue and red dots. (**h**) Regulated Ikaros target genes, which are implicated in pre-BCR signaling (19) or cell adhesion and migration (22) in pro-B cells (Supplementary Fig. 4a,b), are highlighted as orange and green dots, respectively.